ALMA MATER STUDIORUM
UNIVERSITÀ DI BOLOGNA

ARCHIVIO ISTITUZIONALE
DELLA RICERCA

Alma Mater Studiorum Università di Bologna
Archivio istituzionale della ricerca

Photoswitchable NIR-Emitting Gold Nanoparticles

This is the final peer-reviewed author's accepted manuscript (postprint) of the following publication:

Published Version:
Bonacchi, S., Cantelli, A., Battistelli, G., Guidetti, G., Calvaresi, M., Manzi, J., et al. (2016). Photoswitchable NIR-Emitting Gold Nanoparticles. ANGEWANDTE CHEMIE. INTERNATIONAL EDITION, 55(37), 11064-11068 [10.1002/anie.201604290].

Availability:
This version is available at: https://hdl.handle.net/11585/566644.7 since: 2018-11-05

Published:
DOI: http://doi.org/10.1002/anie.201604290

Terms of use:

Some rights reserved. The terms and conditions for the reuse of this version of the manuscript are specified in the publishing policy. For all terms of use and more information see the publisher's website.

This item was downloaded from IRIS Università di Bologna (https://cris.unibo.it/).
When citing, please refer to the published version.

(Article begins on next page)

09 October 2026

This is the peer reviewed version of the following article:

S. Bonacchi, A. Cantelli, G. Battistelli, G. Guidetti, M. Calvaresi, J. Manzi, L. Gabrielli, F. Ramadori, A. Gambarin, F. Mancin, M. Montalti, Angew. Chem. Int. Ed. 2016, 55, 11064.

which has been published in final form at [https://doi.org/10.1002/anie.201604290]

This article may be used for non-commercial purposes in accordance with Wiley Terms and Conditions for Use of Self-Archived Versions.

Photoswitchable NIR emitting gold nanoparticles

Sara Bonacchi,[a] Andrea Cantelli,[a] Giulia Battistelli,[a] Gloria Guidetti,[a] Matteo Calvaresi,[a] Jeannette Manzi,[a] Luca Gabrielli,[b] Federico Ramadori,[b] Alessandro Gambarin,[b] Fabrizio Mancin[b] and Marco Montalti[a]*

Photo-switching of the NIR emission of gold nanoparticles (GNP) upon photo-isomerization of azobenzene ligands, bound to the surface, is demonstrated. Photophysical results prove the occurrence of an excitation energy transfer process from the ligands to the GNP that produces sensitized NIR emission. Because of this process, the excitation efficiency of the gold core, upon excitation of the ligands, is much higher for the trans form than for the cis one and *t*→*c* photo-isomerization causes a relevant decrease of the GNP NIR emission. As a consequence, photo-isomerization can be monitored by ratiometric detection of the NIR emission, upon dual excitation. The photo-isomerization process is followed in real time by detecting, simultaneously, absorbance and luminescence changes, using a dedicated setup. Surprisingly, the photo-isomerization rate of the ligands, bound to the GNP surface, is the same measured, for the same chromophores, in solution. This outcome demonstrates that excitation energy transfer to gold assists photo-isomerization, rather than competing with it. These results pave the road to the development of new, NIR emitting, stimuli responsive nanomaterials for theranostics.

Stimuli-responsive molecular, supramolecular and nanostructured systems are drawing increasing attention, in view of their application in fields of high economic and social impact as material and life sciences.[1] Light [2] offers several advantages compared to other forms of stimulation (e.g. electrical,[3] thermal,[4] pH,[5] pressure,[6] redox).[7] Light beams, in fact, are poorly invasive, remotely addressable and focusable with high spatio-temporal resolution. Moreover, wavelength selection permits, implicitly, multiplexed detection.[8] Additionally, multi-functionality can be easily achieved by combining photo-activatible and photoluminescent components. This approach is typically exploited in nanomedicine to design theranostic nanoparticle (NPs) suitable both as luminescent contrast agents for imaging[9] as well as triggerable vectors for the delivery of therapeutic cargos.[10] For this kind of applications, the development of NPs with tailored emission in the near-infrared region (NIR) is essential, since the transparency of biological tissues is optimal in this spectral window.[11]

Photo-isomerization (PI) of azobenzene[12] (AB) has been widely exploited to control and tune the properties of materials,[13] in order to perform different functions, including drug controlled release.[8b] A large variety of hybrid nano-systems that join the unique optical and electronic properties of gold nanoparticles (**GNP**) to the photochemical activity of AB have been developed.[1c, 13d, 14] Nevertheless, examples of architectures that combine the well documented NIR emission of small (d < 2 nm) **GNP**[15] to the photo-responsivity of AB are very rare[16] and, in particular, the possibility of switching the NIR luminescence of **GNP** upon PI of surface bound AB units has never been demonstrated before.

Here, we report the photophysical and photochemical properties of a newly synthesized class of luminescent **GNP**, stabilized with the AB containing thiolate **A** (scheme 1). Our results demonstrate that, upon excitation of the ligands, sensitized NIR emission of the **GNP** is observed thanks to an efficient energy transfer (ET) process.[17] As a consequence, the NIR luminescence of **GNP** can be switched ON/OFF by alternating UV to blue irradiation. Furthermore, the isomerization state of the NPs can be monitored by ratiometric detection of the NIR luminescence (scheme 1).

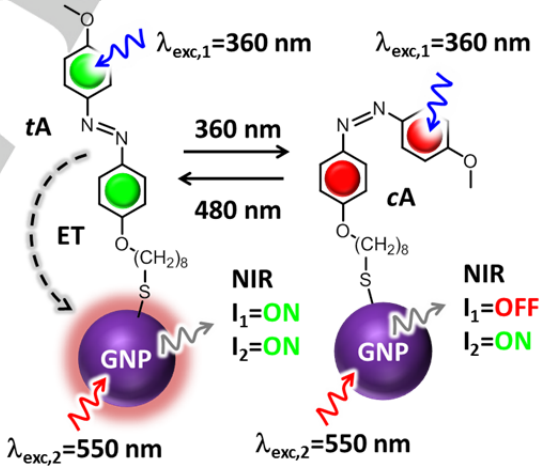

Scheme 1. Chemical formula of the *trans* azobenzene ***t*A** and of its *cis* isomer ***c*A** bound to **GNP**. When the ligands are in the *trans* form (left, ***t*A-GNP**, ON state) ET from ***t*A** to the **GNP** produces NIR sensitized emission upon ligands excitation. Such contribution, due to sensitization, is lost upon PI, in ***c*A** covered NPs (right, ***c*A-GNP**, OFF state).

The thermodynamically stable, **A** *trans* isomer, ***t*A** showed, in $CHCl_3$ solution, the typical absorption band of AB dyes with maximum at 360 nm and $\varepsilon = 2.7 \times 10^4$ M^{-1} cm^{-1}.[12a] A gradual decrease of the intensity of this band was observed, as reported for similar molecules, upon irradiation at 360 nm, because of *t*→*c* PI. At the photo-stationary state (PSS), the absorbance at 360 nm was decreased to about 5% of the initial one. This observation allowed us to conclude that: i) almost complete *t*→*c*

[a] Dr. S. Bonacchi, Dr. A. Cantelli, Dr. G. Battistelli, G. Guidetti, Dr. Matteo Calvaresi, Jeannette Manzi, Prof. M. Montalti
Department of Chemistry "G. Ciamician"
University of Bologna
Via Selmi 2, 40126, Bologna, Italy
E-mail: marco.montalti2@unibo.it
[b] Luca Gabrielli, Dr. F. Ramadori, Dr. A. Gambarin, Prof. F. Mancin
Department of Chemical Sciences
Università degli Studi di Padova
via Marzolo 1, 35131 Padova (Italy)
Supporting information for this article is given via a link at the end of the document.

UNDER PEER REVIEW

conversion occurred at the PSS and ii) the molar absorption coefficient of ***c*A** at 360 nm was negligible with respect to the one of ***t*A**.

Going more into detail, the absorption spectra recorded at different irradiation times (see SI) showed two isosbestic points at 320 nm and 429 nm. This behavior demonstrated that only the two species ***t*A** and ***c*A** were present in the solution, while no side photo-products were formed upon irradiation. Moreover, the absorption spectrum at the PSS practically resembles ***c*A**. This spectrum showed two peaks at 314 nm and 448 nm (ε = 1.0x10^4 M^{-1}cm^{-1} and ε = 3.0x10^3 M^{-1}cm^{-1} respectively). The measured PI quantum yield was $\Phi_{t\text{-}c}$ = 0.15, as reported for analogous AB derivatives.[12a] No fluorescence was observed either for ***t*A** (λ_{exc}=360 nm) or for ***c*A** (λ_{exc}=480 nm).

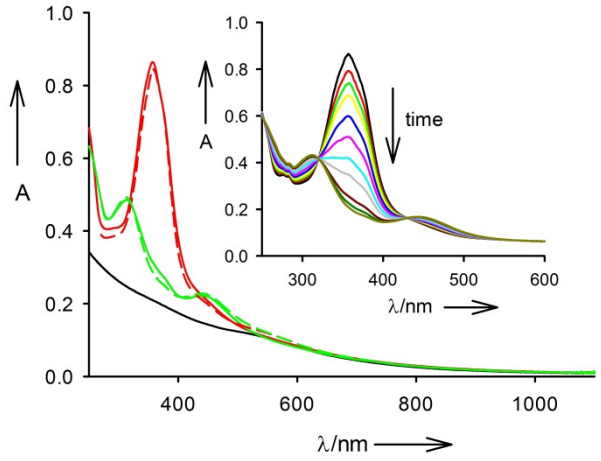

Figure 1. Continuous lines: absorption spectra of the thermodynamically stable ***t*A-GNP** in $CHCl_3$ (red) of the photo-isomerized NPs ***c*A-GNP** (green) and of reference $CH_3(CH_2)_{11}SH$ stabilized **GNP** (black) Dashed lines: linear combinations of the absorption spectrum of the reference **GNP** with those of the ligands ***t*A**. (red) and ***c*A** (green). **Inset.** Absorption spectra of a $CHCl_3$ solution of ***t*A-GNP** during irradiation at 360 nm.

As far as the NPs are concerned, the absorption spectrum of the ***t*A**-coated nanoclusters ***t*A-GNP** (average diameter of the gold core 1.8 nm, estimated formula Au_{144}***t*A**$_{60}$) presented, in $CHCl_3$, both the band at 360 nm of the ***t*A** chromophore and the weak surface plasmon resonance band of the gold core,[18] being the latter one dominant in the region above 550 nm (figure 1). More precisely, the absorption spectrum of ***t*A-GNP** matches the one calculated for Au_{144}***t*A**$_{60}$ as linear combination of the spectra of ***t*A** and of a reference sample of $CH_3(CH_2)_{11}SH$ stabilized **GNP** (figure 1). This spectral matching, and hence the lack of spectral perturbation, proved that electronic interactions between adjacent ***t*A** units, as well as between ***t*A** and the gold core, were weak at the ground state.

In order to investigate the influence of the binding to the **GNP** on the PI $t \rightarrow c$ process, ***t*A-GNP** were irradiated at 360 nm in the same conditions used for the reference compound ***t*A**. As shown in figure 1, the peaks at 314 nm and 448 nm, typical of ***c*A**, were observed at the PSS. Moreover, the same two isosbestic points at 319 nm and 430 nm, observed during the PI of the free ligand ***t*A,** were maintained during the irradiation of ***t*A-GNP**. In particular, at the PSS, the absorption spectrum perfectly matched the one expected in the case of >95% $t \rightarrow c$ conversion. Considered the almost complete PI of the ligands to the cis form NPs at the PSS were labelled as ***c*A-GNP**). The large extent of photoswitching was the result of specific engineering of the ligand, according to studies previously reported for analogous 4,4'-dialcoxiazobenzene derivatives.[19] Interestingly,the PI quantum yield measured for ***t*A-GNP** was $\Phi_{t\text{-}c}$ = 0.15, a value that matched the one observed for the reference compound ***t*A**.

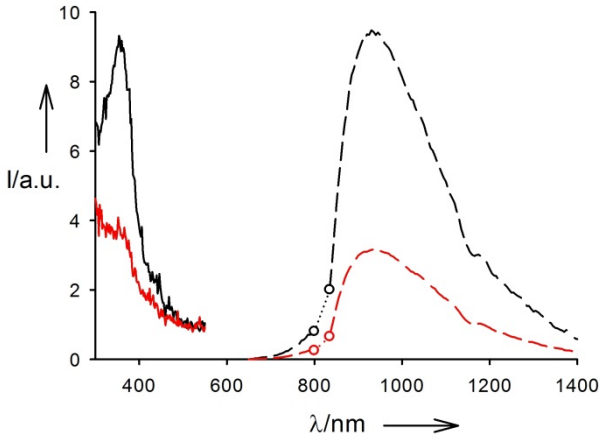

Figure 2. Continuous lines: excitation spectra of the thermodynamically stable ***t*A-GNP** in $CHCl_3$ (black) and of the photo-isomerized NPs ***c*A-GNP** (red). Dashed lines: luminescence spectra (λ_{exc} = 360 nm) of the thermodynamically stable ***t*A-GNP** in $CHCl_3$ (black) and of the photo-isomerized NPs ***c*A-GNP** (red).

As far as luminescence is concerned, a broad emission band in the NIR region, with maximum at about 930 nm, was observed upon excitation of either ***t*A-GNP** or ***c*A-GNP** in $CHCl_3$. The emission spectral profile was, for both the samples, independent on the excitation wavelength, in the 300-600 nm range, and consistent with data reported for similar gold NPs.[15d] In order to investigate the effect of ligand PI on the NIR luminescence, we compared the emission spectra of the same sample of NPs recorded first at the thermodynamically stable state (***t*A-GNP**) and then at the PSS (***c*A-GNP**). The emission spectra acquired upon direct excitation of the gold core ($\lambda_{exc,2}$ = 550 nm, where absorption the ligands is negligible) were identical within the experimental error (see SI). On the contrary, upon excitation at 360 nm, a decrease of about 60% of the intensity of the emission band was observed going from ***t*A-GNP** to ***c*A-GNP** as an effect of the $t \rightarrow c$ PI (figure 2). These observations allowed us to conclude that: i) the emission quantum yield of the gold NP did not change because of the PI, ii) part of the excitation energy adsorbed by ***t*A** was transferred to the gold leading to sensitized emission. Sensitization was confirmed by the excitation spectrum of the NIR emission, shown in figure 2, where the band corresponding to the absorption of ***t*A** was clearly detectable in the ***t*A-GNP**. On the contrary the typical absorption band at 450 nm of the cis form ***c*A** was not observed in the excitation spectrum of the photo-

isomerized NPs *c***A-GNP** (figure 2) revealing a poor contribution due to sensitized emission.

Although the mechanism of excitation ET toward GNP is still debated[20] the poor sensitization observed in the case of *c***A-GNP** is consistent with the following observations. i) *c*A electronic transition centered at 450 nm is forbidden (n-π),[12a] hence its contribution to the overall excitation efficiency of the *c***A-GNP** is minor. ii) MD simulation (see SI) demonstrated that a major fraction of AB molecules are closer to the metal core in *t***A-GNP** than in *c***A-GNP**. iii) Much shorter excited state lifetimes have been reported for the cis than for the trans form.[12a] As a consequence, independently on the model,[20] ET efficiency is expected to be much lower, for the same ET constant rate in the case of *c***A** with respect to *t***A** (See SI).

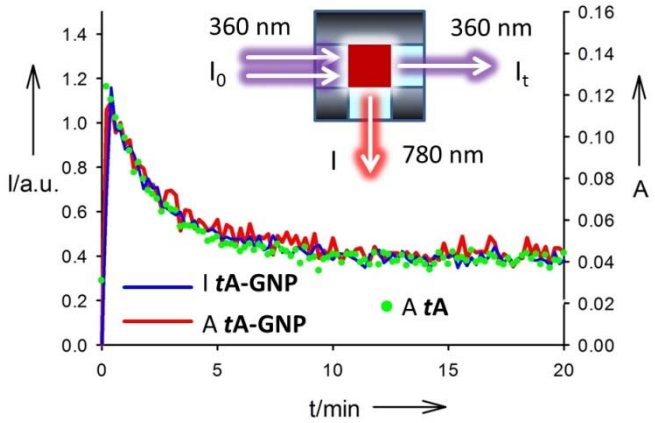

Figure 3. Changes in the photophysical properties of *t***A-GNP** during irradiation at 360 nm in $CHCl_3$. The setup used for the measurements is schematized in the inset. The fraction of irradiation light (I_0) transmitted by the sample I_t is used to measure the absorbance in real time ($A=-\log I_0/I_t$, red line). Luminescence at 780 nm is also measured in real time (I, blue line). The absorbance changes of a $CHCl_3$ solution of *t***A** during irradiation at 360 nm were also measured (green dots).

A dedicated experimental setup, suitable for detecting simultaneously light transmitted and emitted by the NPs samples during irradiation (figure 3, inset), was developed in order to demonstrate, definitively, the correlation between the PI process and the NIR luminescence changes.

Absorbance and emission data recorded for *t***A-GNP** during irradiation were compared with the absorbance values measured for *t***A** in the same conditions (figure 3). The good overlap between the normalized absorbance and luminescence plots for *t***A-GNP** confirmed the correlation between the PI process and the decrease of the luminescence intensity of the **GNP**.

Both absorbance and luminescence plots could be fitted with an exponential decay with a rate constant k = 0.43±0.03 min^{-1}. Interestingly, absorbance changes measured for the reference compound *t***A** showed the same kinetics of *t***A-GNP** (figure 3) with a decay constant k = 0.42±0.03 min^{-1}. These results confirmed that the rate of the t→*c* PI process for *t***A**, bound to the **GNP** surface, was identical to one measured for the molecule free in solution.

Upon irradiation of *c***A-GNP** at 480 nm, *c*→*t* PI occurred and about 70% of *c***A** was converted into *t***A** at the PSS. In order to further investigate the reversibility of the system, we performed a series of PI cycles by detecting the **GNP** emission intensity upon excitation either at $\lambda_{exc,1}$=360 nm or $\lambda_{exc,2}$=550 nm (I_1 and I_2 respectively). Hence, we calculated the concentration independent ratiometric signal I_1/I_2, potentially useful for theranostic application (figure 4, red lines). Regeneration of the *trans* form was achieved by irradiation at $\lambda_{exc,1}$=480 nm (figure 4, blue lines). As shown in figure 4, the NIR emission decreased upon irradiation/excitation at 360 nm. In particular, starting from *t***A-GNP**, an intensity decrease of about 70% was observed in the first 240 s, because of the isomerization of *t***A** and the consequent loss of the sensitized emission. During the following 240 s of irradiation/excitation at 480 nm, the NIR emission intensity increased slightly, since only poor sensitization of the gold emission occurred. After that, 360 nm excitation was restored, and a strong increase of the ratiometric signal, with respect to the final value of the previous UV irradiation cycle, was observed.

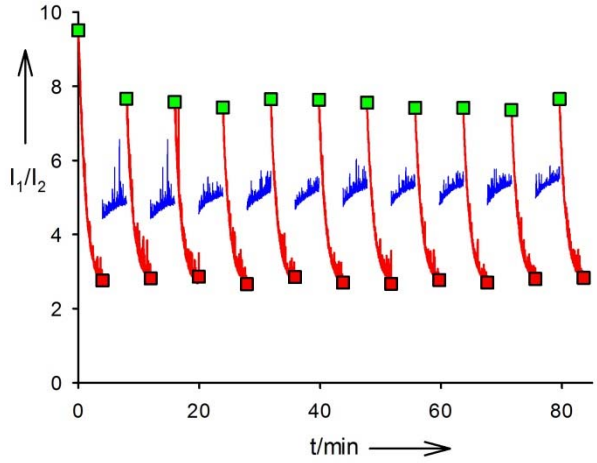

Figure 4. NIR luminescence intensity ratio upon excitation at $\lambda_{exc,1}$ ($\lambda_{exc,1}$ = 360 nm for the red tracks and $\lambda_{exc,1}$ = 480 nm for the blue tracks, intensity I_1 is measured at 780 nm) and $\lambda_{exc,2}$ = 550 (intensity I_2 at 780 nm) of ***t*A-GNP** in $CHCl_3$.Squares show the emission intensity at the beginning (green) and at the end (red) of each irradiation cycle at 360 nm (*t*→*c* PI).

Summarizing, the NIR emission of the **GNP** can be reversibly switched from ON (figure 4, green squares) to OFF (figure 4, red squares) by alternating between UV and Vis irradiation. Moreover, the I_1/I_2 value at $\lambda_{exc,1}$ = 360 nm and $\lambda_{exc,2}$ = 550 nm can be clearly used as an isomerization state indicator.

In conclusion, we demonstrated that PI of the AB derivative *t***A** bound to **GNP** occurred efficiently in our system. The conversion of *t***A-GNP** into *c***A-GNP** took place almost quantitatively (>95%) with a quantum yield identical to the one measured for *t***A** in solution (upon irradiation at 360 nm). Regeneration of 70% of *t***A-GNP** was, in turn, achieved by irradiation of *c***A-GNP** at 480 nm. Photoluminescence measurements showed that *t***A-GNP** emitted in the NIR region upon direct excitation of the gold core ($\lambda_{exc,2}$ = 550 nm) and that,

upon excitation of the *t***A** ligand ($\lambda_{exc,1}$ = 360 nm), an ET process from the molecular ligand to the metal core occurred, producing sensitized NIR emission. Thanks to this process, the ratio of the emission intensity, measured in the two different excitation conditions (either $\lambda_{exc,1}$ or $\lambda_{exc,2}$) could be used to detect the isomerization state of the NPs. Ratiometric detection offer several advantages with respect to single wavelength detection, including concentration independent response. Surprisingly, the lack of any effect of the binding to **GNP** on the PI rate of *t***A** suggested that the ET process to gold assisted the PI rather than competing with it.

Finally, although the typically modest luminescence quantum yield of GNP[15d, 21] needs to be improved to make them competitive with respect to other systems for in-vivo application[11c, 11e, 22] we believe that the results we reported here pave the road to the development of new NIR emitting stimuli responsive nanomaterials for combined diagnostics and therapeutics.

Acknowledgements

The research leading to these results has received funding from the European Union Seventh Framework Programme under grant agreement n°604391 Graphene Flagship. We gratefully acknowledge financial support from ERC (''MOSAIC'' Starting Grant 259014).

Keywords: near infrared • stimuli responsive • nanoparticles • gold • luminescence

[1] a) E. Borre, J. F. Stumbe, S. Bellemin-Laponnaz, M. Mauro, *Angew. Chem. Int. Ed.* **2016**, *55*, 1313-1317; b) G. S. Kumar, D. C. Neckers, *Chem. Rev.* **1989**, *89*, 1915-1925; c) J. Zhang, J. K. Whitesell, M. A. Fox, *Chem. Mater.* **2001**, *13*, 2323-2331; d) A. P. Blum, J. K. Kammeyer, A. M. Rush, C. E. Callmann, M. E. Hahn, N. C. Gianneschi, *J. Am. Chem. Soc.* **2015**, *137*, 2140-2154; e) L. D. Zarzar, J. Aizenberg, *Acc. Chem. Res.* **2014**, *47*, 530-539; f) J.-M. Lehn, *Angew. Chem. Int. Ed.* **2015**, *54*, 3276-3289; g) M. Montalti, G. Battistelli, A. Cantelli, D. Genovese, *Chem. Commun.* **2014**, *50*, 5326-5329; h) H. Kumari, S. R. Kline, S. R. Kennedy, C. Garvey, C. L. Raston, J. L. Atwood, J. W. Steed, *Chem. Commun.* **2016**, *52*, 4513-4516; i) G. O. Lloyd, J. W. Steed, *Nature Chem.* **2009**, *1*, 437-442.

[2] a) S. V. Aradhya, L. Venkataraman, *Nat. Nanotechnol.* **2013**, *8*, 399-410; b) Y. Wu, Y. Xie, Q. Zhang, H. Tian, W. Zhu, A. D. Q. Li, *Angew. Chem. Int. Ed.* **2014**, *53*, 2090-2094; c) S. J. Wezenberg, K.-Y. Chen, B. L. Feringa, *Angew. Chem. Int. Ed.* **2015**, *54*, 11457-11461; d) W. A. Velema, J. P. van der Berg, W. Szymanski, A. J. M. Driessen, B. L. Feringa, *ACS Chem. Biol.* **2014**, *9*, 1969-1974; e) W. A. Velema, J. P. van der Berg, M. J. Hansen, W. Szymanski, A. J. M. Driessen, B. L. Feringa, *Nature Chem.* **2013**, *5*, 924-928.

[3] S. Taccola, F. Greco, E. Sinibaldi, A. Mondini, B. Mazzolai, V. Mattoli, *Adv. Mater.* **2015**, *27*, 1668-1675.

[4] C. A. Figg, A. Simula, K. A. Gebre, B. S. Tucker, D. M. Haddleton, B. S. Sumerlin, *Chem. Sci.* **2015**, *6*, 1230-1236.

[5] M. Kanamala, W. R. Wilson, M. Yang, B. D. Palmer, Z. Wu, *Biomaterials* **2016**, *85*, 152-167.

[6] Y. Wang, X. Tan, Y.-M. Zhang, S. Zhu, I. Zhang, B. Yu, K. Wang, B. Yang, M. Li, B. Zou, S. X.-A. Zhang, *J. Am. Chem. Soc.* **2015**, *137*, 931-939.

[7] K. Miyamae, M. Nakahata, Y. Takashima, A. Harada, *Angew. Chem. Int. Ed.* **2015**, *54*, 8984-8987.

[8] a) D. Bleger, S. Hecht, *Angew. Chem. Int. Ed.* **2015**, *54*, 11338-11349; b) W. A. Velema, W. Szymanski, B. L. Feringa, *J. Am. Chem. Soc.* **2014**, *136*, 2178-2191; c) M. Baroncini, S. d'Agostino, G. Bergamini, P. Ceroni, A. Comotti, P. Sozzani, I. Bassanetti, F. Grepioni, T. M. Hernandez, S. Silvi, M. Venturi, A. Credi, *Nature Chem.* **2015**, *7*, 634-640; d) V. Balzani, G. Bergamini, P. Ceroni, *Angew. Chem. Int. Ed.* **2015**, *54*, 11320-11337.

[9] Z. Tian, A. D. Q. Li, *Acc. Chem. Res.* **2013**, *46*, 269-279.

[10] a) R. Lehner, X. Wang, M. Wolf, P. Hunziker, *J. Controlled Release* **2012**, *161*, 307-316; b) C. Stoffelen, J. Voskuhl, P. Jonkheijm, J. Huskens, *Angew. Chem. Int. Ed.* **2014**, *53*, 3400-3404.

[11] a) V. Shanmugam, S. Selvakumar, C. S. Yeh, *Chem. Soc. Rev.* **2014**, *43*, 6254-6287; b) D. M. Yang, P. A. Ma, Z. Y. Hou, Z. Y. Cheng, C. X. Li, J. Lin, *Chem. Soc. Rev.* **2015**, *44*, 1416-1448; c) M. Montalti, A. Cantelli, G. Battistelli, *Chem. Soc. Rev.* **2015**, *44*, 4853-4921; d) M. Montalti, L. Prodi, E. Rampazzo, N. Zaccheroni, *Chem. Soc. Rev.* **2014**, *43*, 4243-4268; e) E. Rampazzo, F. Boschi, S. Bonacchi, R. Juris, M. Montalti, N. Zaccheroni, L. Prodi, L. Calderan, B. Rossi, S. Becchi, A. Sbarbati, *Nanoscale* **2012**, *4*, 824-830; f) D. Genovese, S. Bonacchi, R. Juris, M. Montalti, L. Prodi, E. Rampazzo, N. Zaccheroni, *Angew. Chem. Int. Ed.* **2013**, *52*, 5965-5968.

[12] a) H. M. D. Bandara, S. C. Burdette, *Chem. Soc. Rev.* **2012**, *41*, 1809-1825; b) S. Castellanos, A. Goulet-Hanssens, F. Zhao, A. Dikhtiarenko, A. Pustovarenko, S. Hecht, J. Gascon, F. Kapteijn, D. Bleger, *Chemistry-a European Journal* **2016**, *22*, 746-752; c) S. Fredrich, R. Goestl, M. Herder, L. Grubert, S. Hecht, *Angew. Chem. Int. Ed.* **2016**, *55*, 1208-1212; d) C.-L. Lee, T. Liebig, S. Hecht, D. Bleger, J. P. Rabe, *ACS Nano* **2014**, *8*, 11987-11993; e) J. Moreno, M. Gerecke, L. Grubert, S. A. Kovalenko, S. Hecht, *Angew. Chem. Int. Ed.* **2016**, *55*, 1544-1547.

[13] a) W. Feng, W. Luo, Y. Feng, *Nanoscale* **2012**, *4*, 6118-6134; b) F. D. Jochum, P. Theato, *Chem. Soc. Rev.* **2013**, *42*, 7468-7483; c) W.-P. Lin, S.-J. Liu, T. Gong, Q. Zhao, W. Huang, *Adv. Mater.* **2014**, *26*, 570-606; d) M. Dobbelin, A. Ciesielski, S. Haar, S. Osella, M. Bruna, A. Minoia, L. Grisanti, T. Mosciatti, F. Richard, E. A. Prasetyanto, L. De Cola, V. Palermo, R. Mazzaro, V. Morandi, R. Lazzaroni, A. C. Ferrari, D. Beljonne, P. Samori, *Nat. Commun.* **2016**, *7*, 11090

[14] a) G. K. Joshi, K. N. Blodgett, B. B. Muhoberac, M. A. Johnson, K. A. Smith, R. Sardar, *Nano Lett.* **2014**, *14*, 532-540; b) G. L. Hallett-Tapley, C. D'Alfonso, N. L. Pacioni, C. D. McTiernan, M. Gonzalez-Bejar, O. Lanzalunga, E. I. Alarcon, J. C. Scaiano, *Chem. Commun.* **2013**, *49*, 10073-10075; c) D. T. Valley, M. Onstott, S. Malyk, A. V. Benderskii, *Langmuir* **2013**, *29*, 11623-11631; d) Y. Q. Yan, J. I. L. Chen, D. S. Ginger, *Nano Lett.* **2012**, *12*, 2530-2536; e) C. Raimondo, B. Kenens, F. Reinders, M. Mayor, H. Uji-i, P. Samori, *Nanoscale* **2015**, *7*, 13836-13839; f) N. Crivillers, S. Osella, C. Van Dyck, G. M. Lazzerini, D. Cornil, A. Liscio, F. Di Stasio, S. Mian, O. Fenwick, F. Reinders, M. Neuburger, E. Treossi, M. Mayor, V. Palermo, F. Cacialli, J. Cornil, P. Samori, *Adv. Mater.* **2013**, *25*, 432-436; g) C. Raimondo, N. Crivillers, F. Reinders, F. Sander, M. Mayor, P. Samori, *Proc. Natl. Acad. Sci. U.S.A.* **2012**, *109*, 12375-12380; h) C. Raimondo, F. Reinders, U. Soydaner, M. Mayor, P. Samori, *Chem. Commun.* **2010**, *46*, 1147-1149.

[15] a) R. Khandelia, S. Bhandari, U. N. Pan, S. S. Ghosh, A. Chattopadhyay, *Small* **2015**, *11*, 4075-4081; b) Z. K. Wu, R. C. Jin, *Nano Lett.* **2010**, *10*, 2568-2573; c) G. L. Wang, T. Huang, R. W. Murray, L. Menard, R. G. Nuzzo, *J. Am. Chem. Soc.* **2005**, *127*, 812-813; d) M. Montalti, N. Zaccheroni, L. Prodi, N. O'Reilly, S. L. James, *J. Am. Chem. Soc.* **2007**, *129*, 2418-2419; e) K. Saha, S. S. Agasti, C. Kim, X. N. Li, V. M. Rotello, *Chem. Rev.* **2012**, *112*, 2739-2779.

[16] Y. Negishi, U. Kamimura, M. Ide, M. Hirayama, *Nanoscale* **2012**, *4*, 4263-4268.

[17] E. Rampazzo, S. Bonacchi, R. Juris, M. Montalti, D. Genovese, N. Zaccheroni, L. Prodi, D. C. Rambaldi, A. Zattoni, P. Reschiglian, *J. Phys. Chem. B* **2010**, *114*, 14605-14613.

[18] a) N. K. Chaki, Y. Negishi, H. Tsunoyama, Y. Shichibu, T. Tsukuda, *J. Am. Chem. Soc.* **2008**, *130*, 8608-8610; b) H. Qian, R. Jin, *Nano Lett.* **2009**, *9*, 4083-4087; c) L. M. Tvedte, C. J. Ackerson, *J. Phys. Chem. A* **2014**, *118*, 8124-8128.

[19] a) J. Dokić, M. Gothe, J. Wirth, M. V. Peters, J. Schwarz, S. Hecht, P. Saalfrank, *J. Phys. Chem. A* **2009**, *113*, 6763-6773; b) C. Dri, M. V. Peters, J. Schwarz, S. Hecht, L. Grill, *Nat Nano* **2008**, *3*, 649-653.

[20] a) T. L. Jennings, M. P. Singh, G. F. Strouse, *J. Am. Chem. Soc.* **2006**, *128*, 5462-5467; b) A. Samanta, Y. D. Zhou, S. L. Zou, H. Yan, Y. Liu, *Nano Lett.* **2014**, *14*, 5052-5057.

[21] Y. Cheng, G. Lu, Y. He, H. Shen, J. Zhao, K. Xia, Q. Gong, *Nanoscale* **2016**, *8*, 2188-2194.

[22] a) Z. Guo, S. Park, J. Yoon, I. Shin, *Chem. Soc. Rev.* **2014**, *43*, 16-29; b) L. Yuan, W. Lin, K. Zheng, L. He, W. Huang, *Chem. Soc. Rev.* **2013**, *42*, 622-661.

WILEY-VCH

COMMUNICATION

Reversible photo-isomerization of azobenenzene ligands bound to the surface of gold nanoparticles (GNP) induces ON/OFF switching of the metal core NIR luminescence. An excitation energy transfer process from the ligands to the GNP, that produces sensitized NIR emission, is at the basis of the phenomenon.

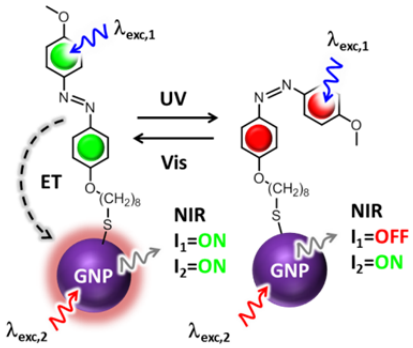

*Sara Bonacchi, Andrea Cantelli, Giulia Battistelli, Gloria Guidetti, Matteo Calvaresi, Jeannette Manzi, Luca Gabrielli, Federico Ramadori, Alessandro Gambarin, Fabrizio Mancin and Marco Montalti**

Page No. – Page No.

Photoswitchable NIR emitting gold nanoparticles

WILEY-VCH

Supporting Information

Photoswitchable NIR emitting gold nanoparticles

Sara Bonacchi,[a] Andrea Cantelli,[a] Giulia Battistelli,[a] Gloria Guidetti,[a] Matteo Calvaresi,[a] Jeannette Manzi,[a] Luca Gabrielli,[b] Federico Ramadori,[b] Alessandro Gambarin,[b] Fabrizio Mancin[b] and Marco Montalti[a]*

[a] Department of Chemistry "G. Ciamician", University of Bologna, Via Selmi 2, 40126, Bologna, Italy e-mail: marco.montalti2@unibo.it

[b] Department of Chemical Sciences Università degli Studi di Padova via Marzolo 1, 35131 Padova (Italy).

Table of Contents

1. Experimental procedures S2
2. Synthesis of thiol ***t*A** S3
3. Synthesis and characterization of nanoparticles ***t*A-GNPs** S7
4. Photophysical measurements. S9
5. Photoisomerization experiments S10
6. Photoisomerization kinetic model S11
7. ^{1}H, ^{13}C and IR and HRMS spectra of the synthesized compounds S16
8. MD simulations: computational details S27
9. Energy-transfer models S29
10. References S30

1. Experimental Procedures.

General: Solvents were purified by standard methods. All commercially available reagents and substrates were used as received.

TLC analyses were performed using Merck 60 F_{254} precoated silica gel glass plates. Column chromatography was carried out on Macherey-Nagel silica gel 60 (70-230 mesh).

NMR spectra were recorded using a Bruker AV III 500 spectrometer operating at 500 MHz for ^{1}H, 125.8 MHz for ^{13}C. Chemical shifts are reported relative to internal Me4Si. Multiplicity is given as follow: s = singlet, d = doublet, t = triplet, q = quartet, qn = quintet, m = multiplet, br = broad peak.

HRMS mass spectra were obtained with an Mariner Applied Biosystem (API-TOF) mass spectrometer (MeOH, 0.5% formic acid).

Melting temperatures were measured using a Stuart SMP10 apparatus.

Elemental analysis were performed with a Perkin-Elmer 2400 CHN microanalyzer.

IR spectra were obtained using a Nicolet 5700 FT-IR spectrometer.

TEM images were recorded on a Jeol 300 PX electron microscope. One drop of sample was placed on the sample grid and the solvent was allowed to evaporate. UV-Visible spectra and kinetic traces were recorded on Cary 50 spectrophotometer equipped with thermostated multiple cell holders. Thermogravimetric analysis (TGA) was run on 1-2 mg nanoparticle samples using a Q5000 IR model TA instrument from 30 to 1000 °C under a continuous air flow.

2. Synthesis of 8-(4-((4-methoxyphenyl)diazenyl)phenoxy)octyl-thiol (*t*A)

The azobenzyl-thiol derivative ***t*A** has been prepared according to the following scheme:

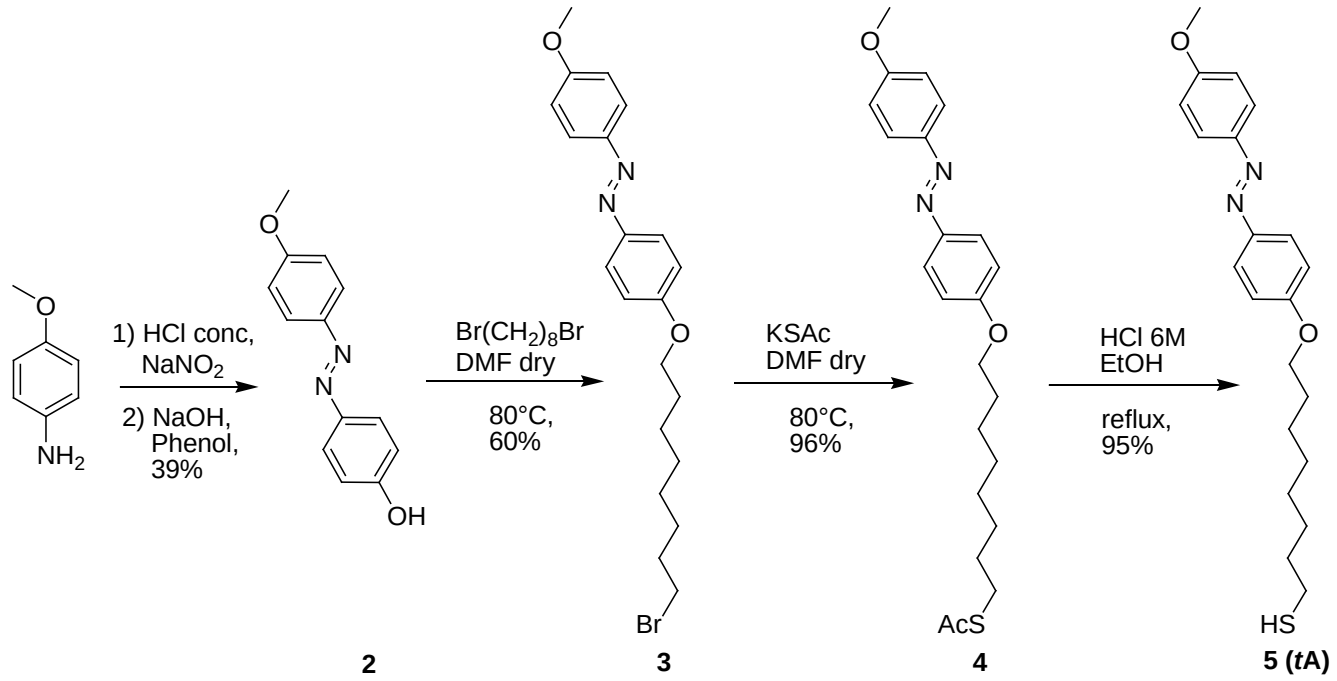

Scheme S1. Synthesis of the azobenzene derivative ***t*A**

2.1 Synthesis of 4-((4-methoxyphenyl)diazenyl)phenol (2)

1.6 g (12.993 mmol, 1 equiv) of *p*-anisidine are dissolved in 30 mL of milliQ water, then the solution is cooled to 0° C in an ice bath and 6 mL of concentrated HCl are added dropwise. Subsequently, 896 mg of $NaNO_2$ (12.993 mmol, 1 equiv) are added and the reaction is stirred for 1 h at 0°C . Then, 1.22 g of phenol (12.993 mmol, 1 equiv), dissolved in 20 mL of a 2.5 M NaOH solution in water, are added. The mixture is stirred for 15 minutes, then the precipitate is filtered off and washed with 5 mL of H_2O, obtaining 1.13 g (yield 39 %) of product **2**. Data are in agreement with those reported in literature.[1]

^{1}H NMR (500 MHz, MeOD) δ 7.83 (d, *J* = 9.0 Hz, 4H, H Ar), 7.78 (d, *J* = 8.8 Hz, 4H, H Ar), 7.04 (d, *J* = 9.0 Hz, 4H, H Ar), 6.92 (d, *J* = 8.8 Hz, 4H, H Ar), 3.87 (s, 3H, C*H*$_3$O).

^{13}C NMR (126 MHz, MeOD) δ 161.8 (1C, C_{quat} Ar), 160.2 (1C, C_{quat} Ar), 146.8 (1C, C_{quat} Ar), 146.0 (1C, C_{quat} Ar), 124.2 (1C, C Ar), 123.8 (1C, C Ar), 115.3 (1C, C Ar), 113.9 (1C, C Ar), 54.7(1C, *C*H$_3$O).

2.2 Synthesis 1-(4-((8-bromooctyl)oxy)phenyl)-2-(4-methoxyphenyl)diazene (3)

750 mg (3.286 mmol, 1 equiv) of compound **2** are dissolved in 5 mL of dry DMF, then 2.42 mL of 1,8-dibromoctane (13.144 mmol, 4 equiv) and 1.8 g of K_2CO_3 (13.144 mmol, 4 equiv) are added. The mixture is stirred under N_2 at 80°C for 5 hours. The solvent is then removed by evaporation at reduced pressure and the reaction crude is extracted in DCM/H_2O; the organic phases are collected, dried over Na_2SO_4 and the solvent is removed under reduced pressure. Purification by flash chromatography (Exane : DCM from 5:5 to 4:6), gives 825 mg (60% yield) of product **3**.

^{1}H NMR (500 MHz, $CDCl_3$) δ 7.94 – 7.87 (m, 4H, H Ar), 7.06 – 6.99 (m, 4H, H Ar), 4.06 (t, *J* = 6.5 Hz, 2H, C*H*$_2$OPh), 3.91 (s, 2H, C*H*$_3$O), 3.44 (t, *J* = 6.8 Hz, 2H, C*H*$_2$Br), 1.94 – 1.87 (m, 2H, CH_2), 1.87 – 1.79 (m, 2H, CH_2), 1.55 – 1.45 (m, 4H, CH_2), 1.44 – 1.36 (m, 4H, CH_2).

^{13}C NMR (126 MHz, $CDCl_3$) δ 161.6 (1C, C_{quat} Ar), 161.2 (1C, C_{quat} Ar), 147.0 (1C, C_{quat} Ar), 146.9 (1C, C_{quat} Ar), 124.4 (1C, C Ar), 124.4 (1C, C Ar), 114.7 (1C, C Ar), 114.2 (1C, C Ar), 68.2 (1C, *C*H$_2$OPh), 55.6 (1C, *C*H$_3$O), 34.0 (1C, *C*H$_2$Br), 32.8 (1C, *C*H$_2$), 29.2(1C, *C*H$_2$), 28.7(1C, *C*H$_2$), 28.1 (1C, *C*H$_2$), 25.9 (1C, *C*H$_2$).

TOF ES$^+$ HRMS: [M+H$^+$] calcd. for $C_{21}H_{28}BrN_2O_2$ = 419.1329. Found = 419.1320.

IR ν (KBr): 2941, 1601, 1581, 1500, 1249, 1146, 844, 548 cm^{-1}.

Melting Point: 98÷99°C

Elemental anal. Calcd for $C_{21}H_{27}BrN_2O_2$ = C, 60.27; H, 6.51; N, 6.70. Found = C, 60.52; H, 6.52; N, 6.70.

2.3 Synthesis of 8-(4-((4-methoxyphenyl)diazenyl)phenoxy)octyl)thioacetate (4)

Compund **3** (710 mg, 1.693 mmol, 1 equiv) is dissolved in 8 mL of dry DMF, then potassium thioacetate (580 mg, 5.079 mmol, 3 equiv) is added. The reaction mixture is stirred at 80°C under N_2 atmosphere for 4 hours. Then the solvent is removed by evaporation at reduced pressure and the residue is purified by flash chromatography (Exane : DCM from 5:5 to 100% DCM) obtaining 670 mg (96% of yield) of product **4**.

^{1}H NMR (500 MHz, $CDCl_3$) δ 7.93 – 7.87 (m, 4H, H Ar), 7.02 (dd, *J* = 8.8, 7.8 Hz, 4H, H Ar), 4.05 (t, *J* = 6.5 Hz, 2H, C*H*$_2$OPh), 3.90 (s, 3H, C*H*$_3$O), 2.90 (t, *J* = 7.3 Hz, 2H, C*H*$_2$S), 2.35 (s, 3H, C*H*$_3$COS), 1.89 – 1.79 (m, 2H, C*H*$_2$), 1.64 – 1.55 (m, 2H, C*H*$_2$), 1.53 – 1.44 (m, 2H, C*H*$_2$), 1.45 – 1.32 (m, 6H, C*H*$_2$).

^{13}C NMR (126 MHz, $CDCl_3$) δ 196.06 (1C, CH_3*C*OS), 161.5 (1C, C_{quat} Ar), 161.2 (1C, C_{quat} Ar), 147.1 (1C, C_{quat} Ar), 146.9 (1C, C_{quat} Ar), 124.4 (1C, C Ar), 124.3 (1C, C Ar), 114.7 (1C, C Ar), 114.2 (1C, C Ar), 68.3 (1C, *C*H_2OPh), 55.6 (1C, *C*H_3O), 30.7 (1C, *C*H_2S), 29.5(1C, *C*H_2), 29.2 (1C, *C*H_2), 29.2 (1C, *C*H_2), 29.1 (1C, *C*H_2), 29.0 (1C, *C*H_2), 28.7 (1C, *C*H_2), 25.9 (1C, *C*H_2).

TOF ES$^+$ HRMS: [M+H$^+$] calcd. for $C_{23}H_{31}N_2O_3S$ = 415.2050. Found = 415.2032.

IR: ν (KBr): 2927, 1683, 1601, 1581, 1248, 1121, 1106 cm^{-1}.

Melting Point: 106÷107°C

Elemental anal. Calcd for $C_{23}H_{30}N_2O_3S$ = C, 66.64; H, 7.29; N, 6.76; S, 7.73. Found = C, 66.51; H, 7.66; N, 6.66; S, 7.76.

2.4 Synthesis of 8-(4-((4-methoxyphenyl)diazenyl)phenoxy)octyl)thiol (5/*t*A)

Compound **4** (200 mg, 0.482 mmol) is suspended in 8 mL of a EtOH : HCl 6M 1:1 mixture, and the reaction is refluxed under N_2 atmosphere for 3 hours. Then the solvent is evaporated under reduced pressure and subsequent purification by flash chromatography (100% DCM) gives the final thiol **5** (170 mg, 95% yield)

^{1}H NMR (500 MHz, $CDCl_3$) δ 7.96 – 7.90 (m, 4H, H Ar), 7.06 – 6.99 (m, 4H, H Ar), 4.06 (t, *J* = 6.5 Hz, 2H, C*H*$_2$OPh), 3.91 (s, 3H, OC*H*$_3$), 2.56 (dd, *J* = 14.7, 7.5 Hz, 2H, C*H*$_2$S), 1.88 – 1.80 (m, 2H, C*H*$_2$), 1.68 – 1.60 (m, 2H, C*H*$_2$), 1.54 – 1.47 (m, 2H, C*H*$_2$), 1.46 – 1.31 (m, 6H, C*H*$_2$).

^{13}C NMR (126 MHz, $CDCl_3$) δ 161.8 (1C, C_{quat} Ar), 161.4 (1C, C_{quat} Ar), 146.6 (1C, C_{quat} Ar), 146.5 (1C, C_{quat} Ar), 124.6 (1C, C Ar), 124.5 (1C, C Ar), 114.8 (1C, C Ar), 114.3 (1C, C Ar), 68.3 (1C, *C*H_2OPh), 55.6 (1C, *C*H_3O), 34.0 (1C, *C*H_2SH), 29.3 (1C, *C*H_2), 29.2 (1C, *C*H_2), 29.0 (1C, *C*H_2), 28.3 (1C, *C*H_2), 26.00 (1C, *C*H_2), 24.6 (1C, *C*H_2).

TOF ES$^+$ HRMS: [M+H$^+$] calcd. for $C_{21}H_{29}N_2O_2S$ = 373.1944. Found = 373.1960.

IR: ν (KBr): 2924, 1601, 1582, 1501, 1246, 1147, 1021, 849 cm^{-1}.

Melting Point: 93÷94°C

Elemental anal. Calcd for $C_{21}H_{28}N_2O_2S$ = C, 67.71; H, 7.58; N, 7.52; S, 8.61. Found = C, 67.68; H, 8.05; N, 7.25; S, 8.36.

3. Synthesis and characterization of monolayer protected gold nanoparticles (*t*A-GNPs)

Monolayer protected gold nanoparticles (***t*A-GNPs**) were prepared according to a previously reported two-step procedure. [2]All the glassware used in the ***t*A-GNPs** preparation was washed with aqua regia and rinsed with distilled water. $HAuCl_4$ is strongly hygroscopic and was weighted within a dry-box.

A solution of $HAuCl_4 \cdot 3H_2O$ (100 mg, 0.254 mmol) in water (4 mL) was extracted with a solution of tetraoctylammonium bromide (5 g, 9.14 mmol) in N_2 purged toluene (250 mL). To the resulting reddish-orange organic solution, dioctylamine (3.36 g, 13.92 mmol) is added (the amount of dioctylamine was calculated[2] in order to obtain 2 nm nanoparticles). The mixture is vigorously stirred under N_2 for 30 min. During this period of time the color of the mixture fades. A solution of $NaBH_4$ (93.0 mg, 2.46 mmol) in H_2O (1 mL) is then rapidly added. The color of the solution turns rapidly to black due to nanoparticles formation. After 2 hours of stirring, the aqueous layer is removed. To the above nanoparticle solution, thiol ***t*A** (0.254 mmol) dissolved in 3 mL of isopropanol is rapidly added. The reaction mixture is evaporated and the resulting crude is dissolved in CH_2Cl_2 and purified by gel permeation chromatography with Biorad Bio-Beads S-X1 resin.

3.1. Characterization of *t*A-GNPs

TEM analysis of the different samples of small nanoparticles (Figure S1) yields an average diameter for the MPGN of 1.7±0.6 nm.

Formula for ***t*A-GNPs** calculate on the basis of TEM diameter and TGA analysis is $Au_{152}RS_{62}$, in agreement with the well-known $Au_{144}RS_{60}$ nanocluster which likely constitutes the majority of the nanoparticles in the sample.[3] TGA analysis of a sample of ***t*A-GNPs** under air atmosphere is shown in

Figure S2. NMR analysis (Figure S3) indicates monolayer formation (broadening of all signals), as confirmed by diffusion-filtered experiments (not shown).

UV-Vis spectrum of figure 1 (main text) confirms the GNPs composition. The spectrum was recorded for a solution prepared by dissolving 0.9 mg ***t*A-GNPs** in 50 ml of $CHCl_3$ ($c_{tA\text{-}GNP}$ = 18 μg ml^{-1}). The concentration of ***tA*** in the solution was hence calculated according to the Lambert-Berr law A = εbc (where A is the absorbance, ε is the molar absorption coefficient, c is the concentration and b = 1 cm is the optical path) to be $2.2x10^{-5}$ M and hence 8 μg ml^{-1}. The gold concentration was hence 10 μg ml^{-1} corresponding to 5.0 $x10^{-5}$M. The molar Au/ligand ratio was hence 2.3 (2.4 expected for Au_{144}***tA***$_{60}$). Moreover the absorption at 510 nm is consistent with the reported molar absorption coefficient for Au_{144} (ε_{510}=$4.34x10^{-5}$ M)[4] being the molecular weight of Au_{144}***tA***$_{60}$ MW= 50756 g/mol.

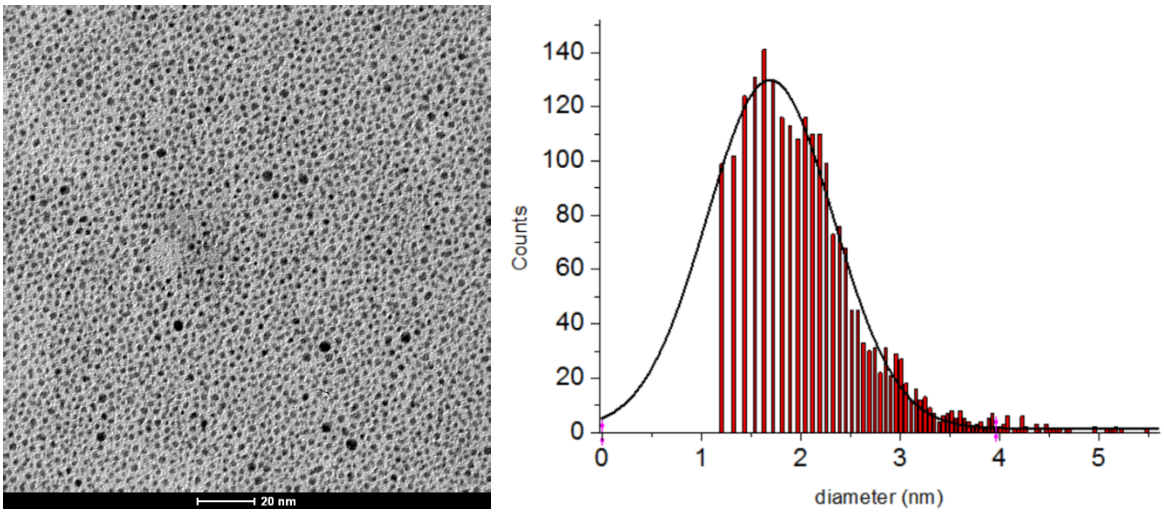

Figure S1: Sample TEM image of ***t*A-GNPs** and size distribution: average diameter = 1.7 nm (σ= 0.6 nm).

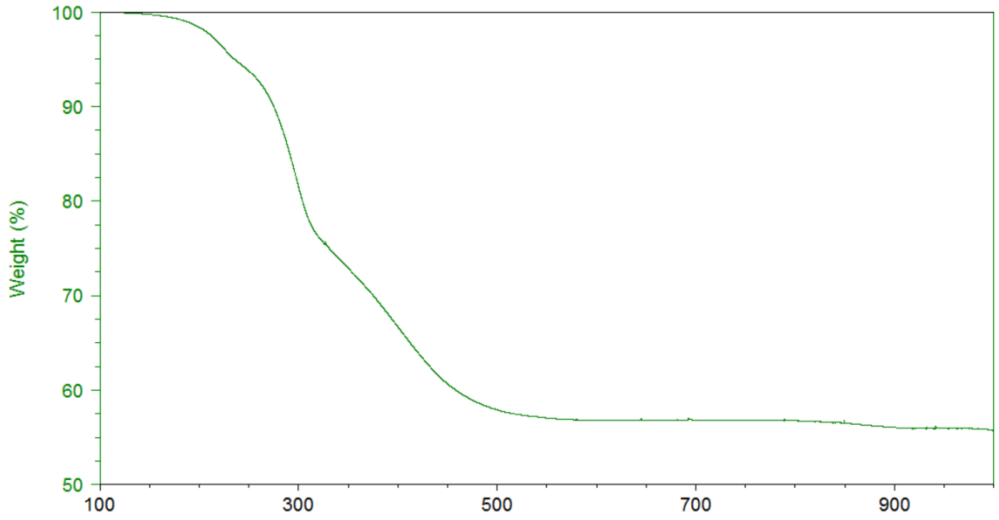

Figure S2: TGA analysis of a sample of ***t*A-GNPs** under air atmosphere.

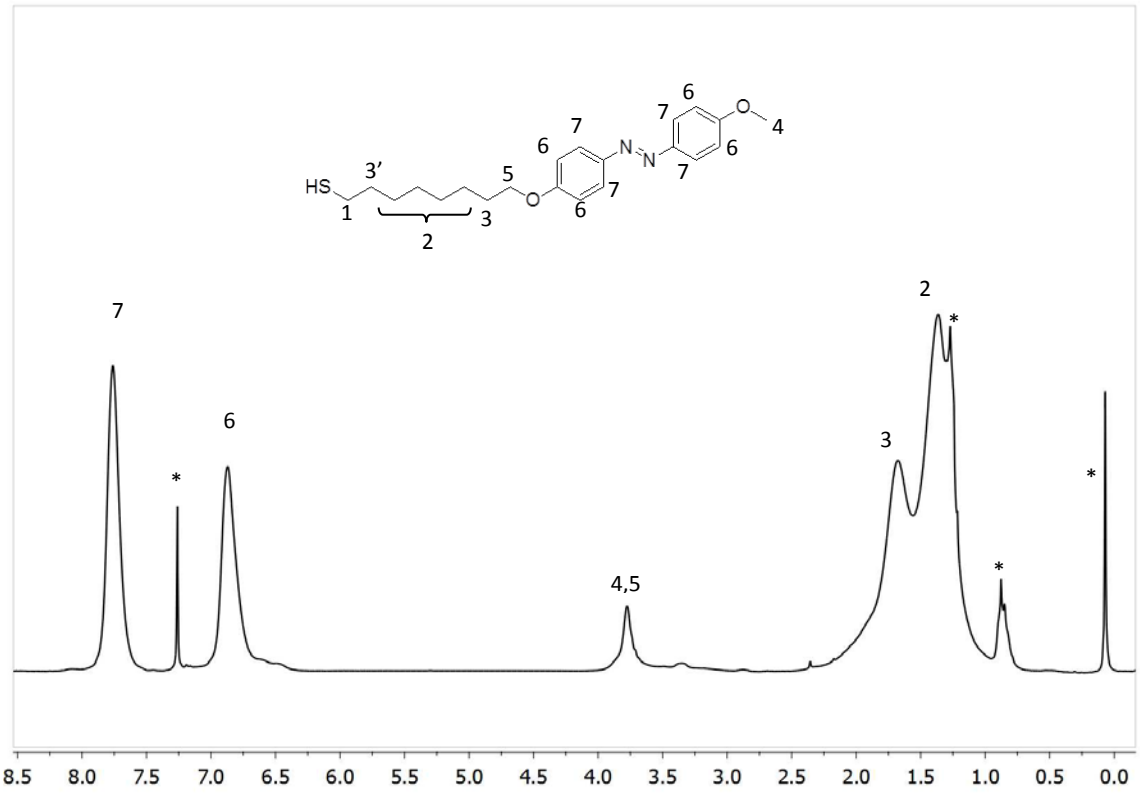

Figure S3: ^{1}H-NMR (300 MHz) spectrum of the ***t*A-GNPs** in $CDCl_3$ (* indicates the residual solvents and impurities). Signals from methylenes 1 and 3' are likely undetectable due to strong line broadening due to their closeness to nanoparticle surface.

4. Photophysical measurements.

All photophysical measurement were performed in air-equilibrated chloroform solution (Merk Uvasol) UV-VIS absorption spectra were performed at 298 K by means of Perkin-Elmer Lambda 45 spectrophotometer. Quartz cuvette with optical path length of 1 cm were used (Hellma). The estimated experimental errors are: 2 nm on the band maximum, 5% on the molar absorption coefficient.

The luminescence spectra were recorded with a spectrofluorimeter Edinburgh FLS920 equipped with a photomultiplier Hamamatsu R928P for the visible region and a a Ge detector for emission in the NIR spectral region. Correction of the emission spectra for detector sensitivity in the 700−1200 nm spectral region was performed.[5]

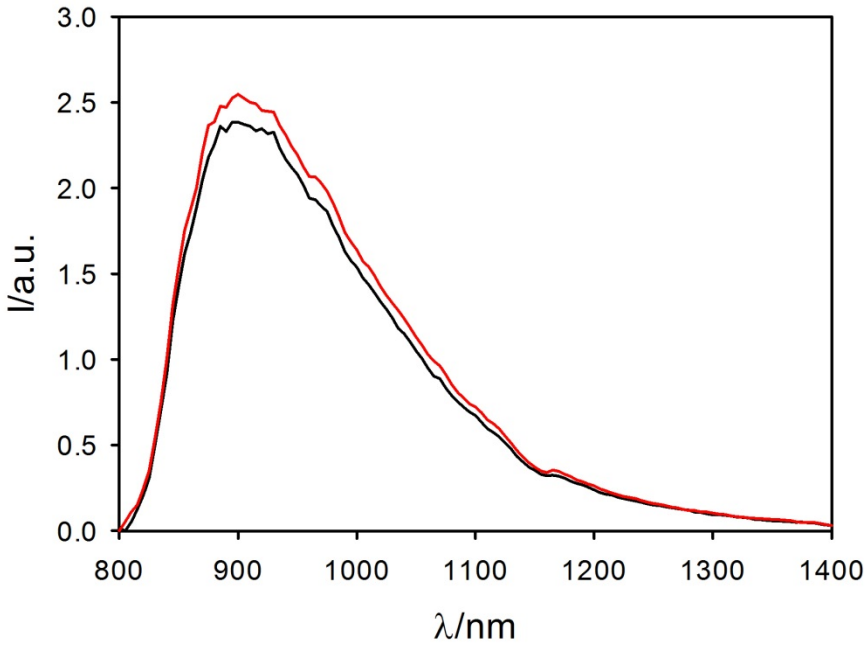

Figure S4 Luminescence spectra (λ_{exc}=550 nm) of the thermodynamically stable ***t*A-GNP** in $CHCl_3$ (red line) and of the photo-isomerized NPs ***c*A-GNP** (black).

5. Photoisomerization experiments.

Photochemical experiments were performed in air-equilibrated chloroform solution (Merk Uvasol). Irradiation at 360 and 480 nm were performed in a spectrofluorimeter Edinburgh FLS920 equipped with a 450 W Xenon lamp. Irradiation wavelength was selected by positioning the excitation monochromator and using 10 nm band-pass slits. The irradiated solution was contained in a spectrophotometric cell (1 cm or 0.3 cm path) and magnetically stirred continuously. The intensity of the incident photon flux was measured by the ferrioxalate actinometer. [5]

The estimated experimental errors are: 10% on the photoreaction quantum yield, 5% on the composition of the photostationary state.

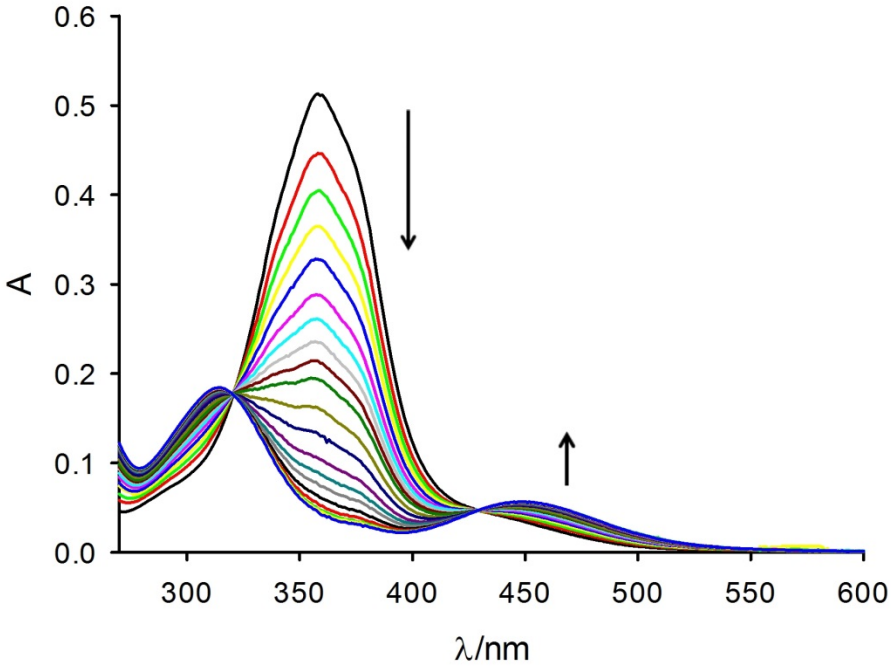

Figure S5 Absorption spectra of a $2x10^{-5}$M solution of ***t*A** in $CHCl_3$ during irradiation at 360 nm.

6. Photoisomerization kinetic model

The trans azobenzene (T) photo-isomerization[6] quantum yield $\phi_T$is the ratio between the number of isomerized T molecules per time unit and the number of photons adsorbed by T per time unit. [5]

$$\phi_T = \frac{-d[T]}{I_0 f_T dt} V$$

[Eq. 1]

Where I_0Is the number of incident photon for time unit, f_T is the fraction of incident photon absorbed by T and V is the solution volume. Photoisomerization of T produces the cis form (C) according to the process:

$$T^* \rightarrow C$$

If irradiation wavelength is suitable to excite the produced C its photoisomerization occours according to the process:

$$C^* \rightarrow T$$

The C photo-isomerization quantum yield $\phi_C$is defined analogously to the one of T:

$$\phi_C = \frac{-d[C]}{I_0 f_C dt} V$$

[Eq. 2]

Where f_T is the fraction of incident photon absorbed by C.

In general for a solution containing i species the fraction of light absorbed by each species f_i can be calculated knowing its contribution A_i, to the absorbance A or its molar absorption coefficient ε_i and the optical path b:

$$A = \sum_i A_i = \sum_i b\varepsilon_i[i]$$

$$f_i = \frac{1 - 10^{-A}}{A} A_i = \frac{1 - 10^{-A}}{A} b\varepsilon_i[i]$$

[Eq. 3]

Considering that in the absence of other photochemical process:

$$[T] + [C] = cost = c_0$$

and hence:

$$\frac{d[T]}{dt} = \frac{-d[C]}{dt}$$

The combination of Eq. 1, 2 and 3 gives the following isomerization rate equation: [5]

$$\frac{d[C]}{dt} = \frac{bI_0}{V}\frac{(1-10^{-A})}{A}\phi_T\varepsilon_T(c_0 - [C]) - \frac{bI_0}{V}\frac{(1-10^{-A})}{A}\phi_c\varepsilon_C[C]$$

[Eq. 4]

At the photostationary state (reached at $t \to \infty$) $[C] = [C]_\infty$ and $d[C]/dt = 0$, hence:

$$\phi_c = \frac{\varepsilon_T(c_0 - [C]_\infty)}{\varepsilon_C[C]_\infty}\phi_T$$

Which can be replaced in eq. 4 giving:

$$\frac{d[C]}{dt} = \frac{bI_0}{V}\frac{(1-10^{-A})}{A}\phi_T\varepsilon_T c_0(1 - \frac{[C]}{[C]_\infty})$$

[Eq. 5]

As far as the absorbance is concerned, for the azobenzene functionalized GNP where the contribution of the gold to the total absorbance is A_G becomes:

$$A = \varepsilon_T b(c_0 - [C]) + \varepsilon_C b[C] + A_G = b(\varepsilon_C - \varepsilon_T)[C] + \varepsilon_T b c_0 + A_G$$

$$A = b(\varepsilon_C - \varepsilon_T)[C] + A_0$$

And hence:

$$[C] = \frac{A - A_0}{b(\varepsilon_C - \varepsilon_T)} \; ; \; \frac{d[C]}{dt} = \frac{1}{b(\varepsilon_C - \varepsilon_T)}\frac{dA}{dt}$$

[Eq. 6]

The combination of Eq. 5 and Eq. 6 gives:

$$\frac{dA}{dt} = \frac{I_0}{V}\frac{(1-10^{-A})}{A}\phi_T\varepsilon_T c_0[b(\varepsilon_C - \varepsilon_T) - \frac{A - A_0}{[C]_\infty}]$$

[Eq. 7]

At the photostationary state (reached at $t \to \infty$) $dA/dt = 0$

$$b(\varepsilon_C - \varepsilon_T) = \frac{A_\infty - A_0}{[C]_\infty}$$

And hence assuming $y_\infty = [C]_\infty / c_0$ Eq. 7 becomes:

$$\frac{dA}{dt} = -\frac{I_0}{V}\frac{(1 - 10^{-A})}{A y_\infty}\phi_T \varepsilon_T (A - A_\infty)$$

[Eq. 8]

Which can be integrated to give:

$$ln\frac{A - A_\infty}{A_\infty - A_0} = -\frac{I_0}{V y_\infty}\phi_T \varepsilon_T \int_0^t \frac{(1 - 10^{-A})}{A} dt$$

Defining:

$$x = \int_0^t \frac{(1 - 10^{-A})}{A} dt; B = \frac{I_0}{V y_\infty}\varepsilon_T$$

[Eq. 9]

Equation 8 becomes:

$$ln\frac{A - A_\infty}{A_\infty - A_0} = -B\phi_T x$$

[Eq. 10]

The variable x was integrated numerically; all the factors composing the term B where known (I_0 was measured by the ferrioxalate actinometer). [5]

The linear fitting of the experimental data $ln\frac{A-A_\infty}{A_\infty-A_0}$ shown in figure S5 allowed us to determine ϕ_T

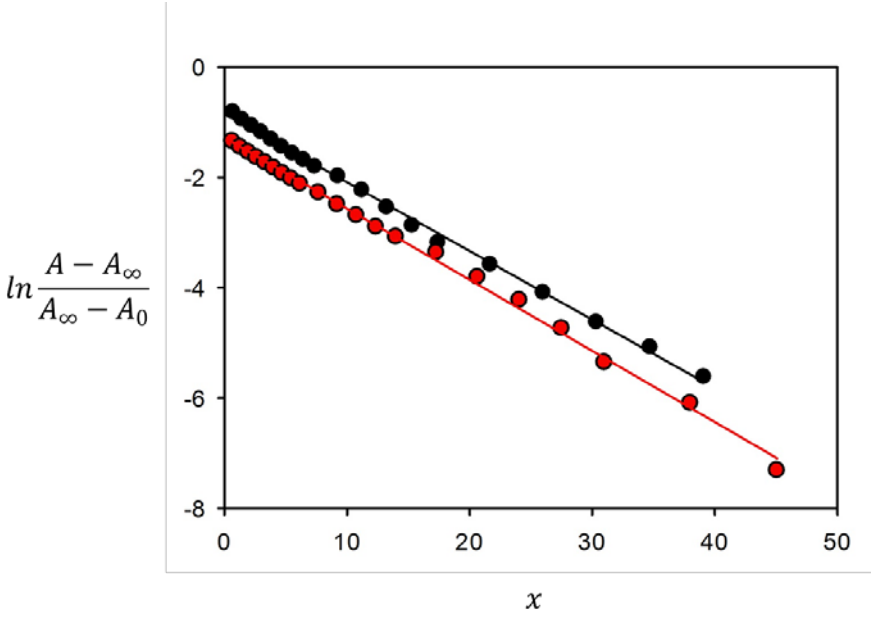

Figure S6 Linear fitting of the absorbance at λ=360 nm as a function of the coordinate x of equation 9 for the azobenzene derivative tA (black dots) and for the functionalized NPs (red dots). The fitting results were used to calculate the $\phi_T$values reported in the main article according to eq. 10.

7. ^{1}H, ^{13}C-NMR and IR and HRMS spectra of the synthesized compounds

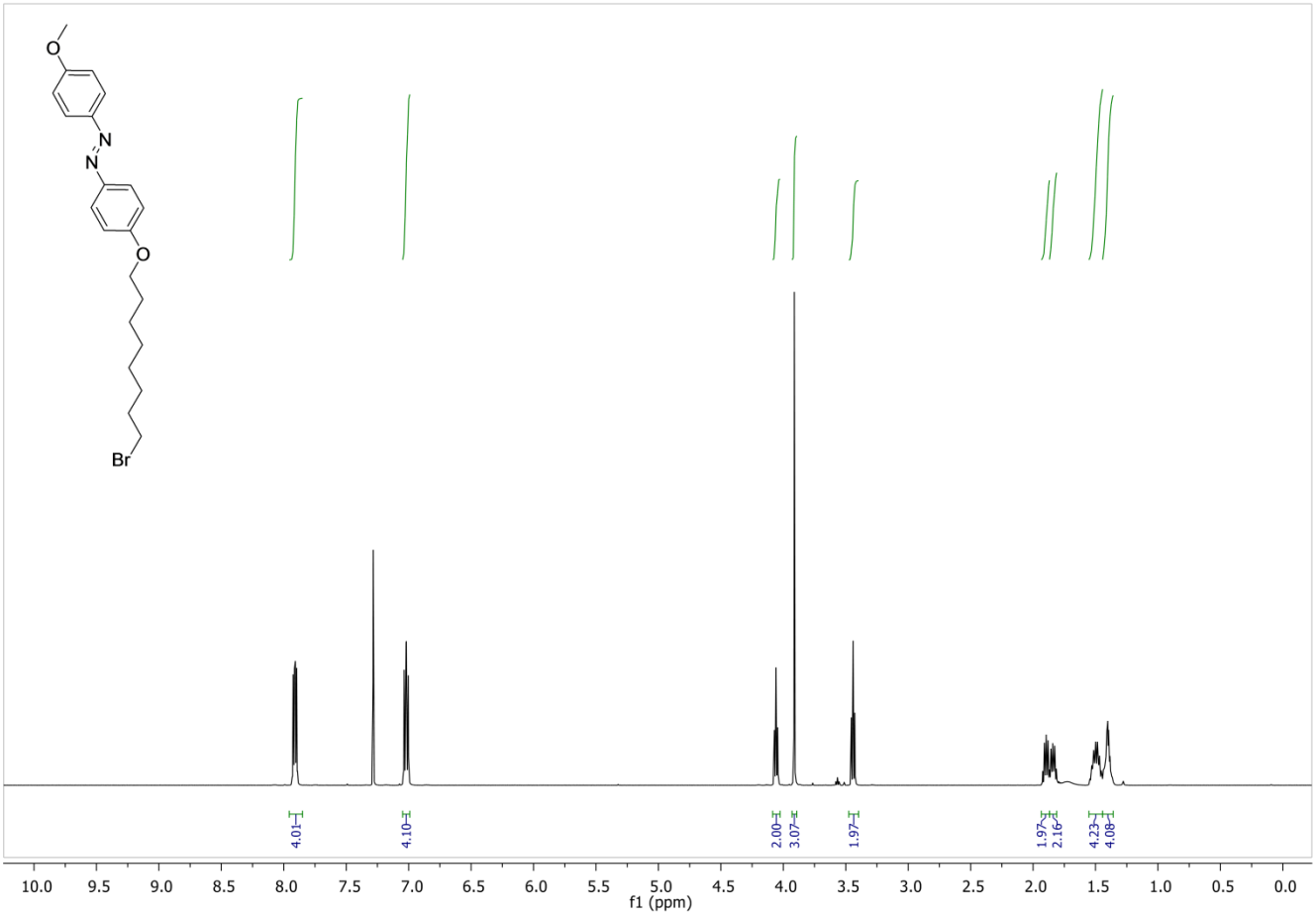

Figure S7 ^{1}H-NMR spectra of compound **3** ($CDCl_3$).

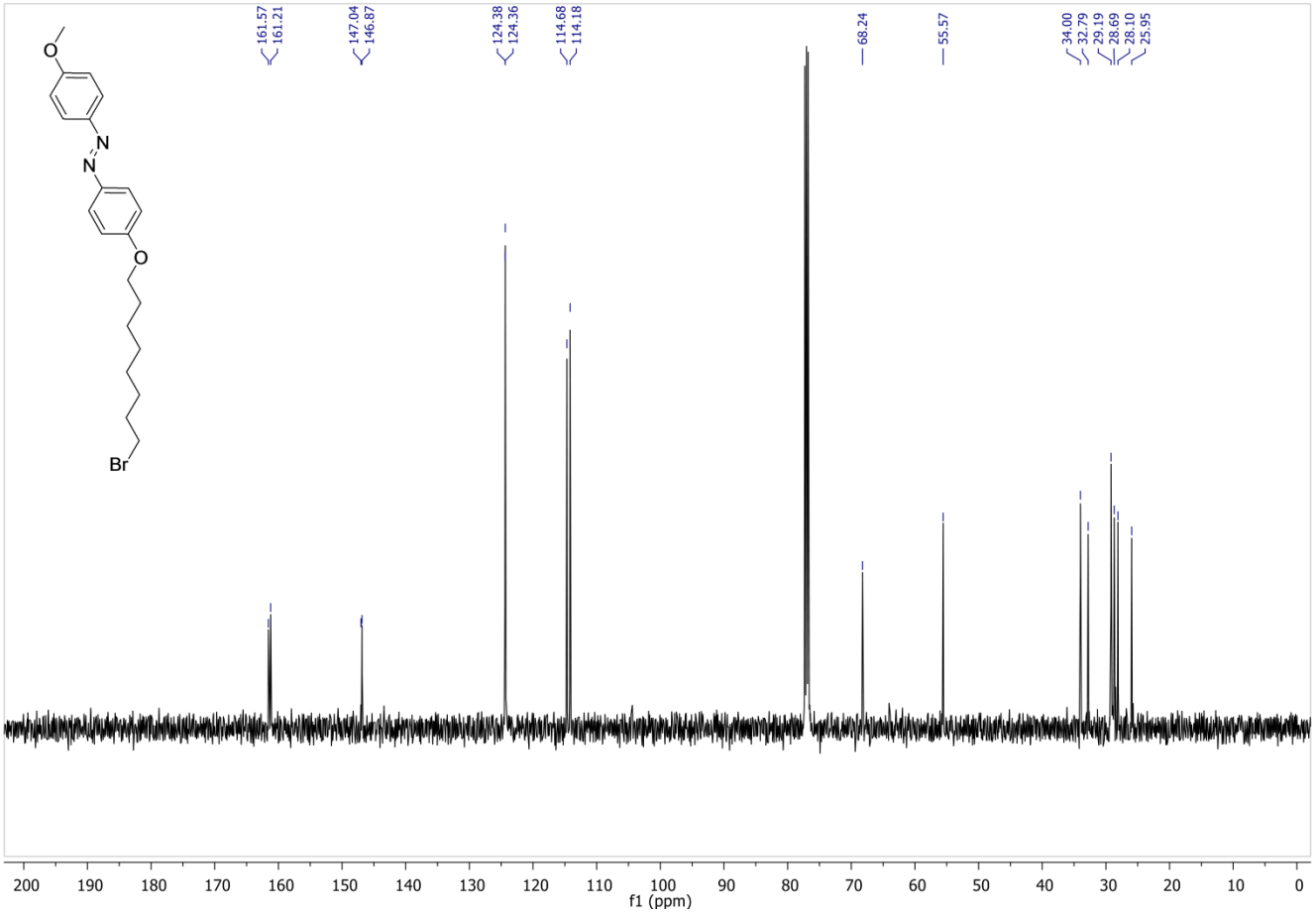

Figure S8 ^{13}C-NMR spectra of compound **3** ($CDCl_3$).

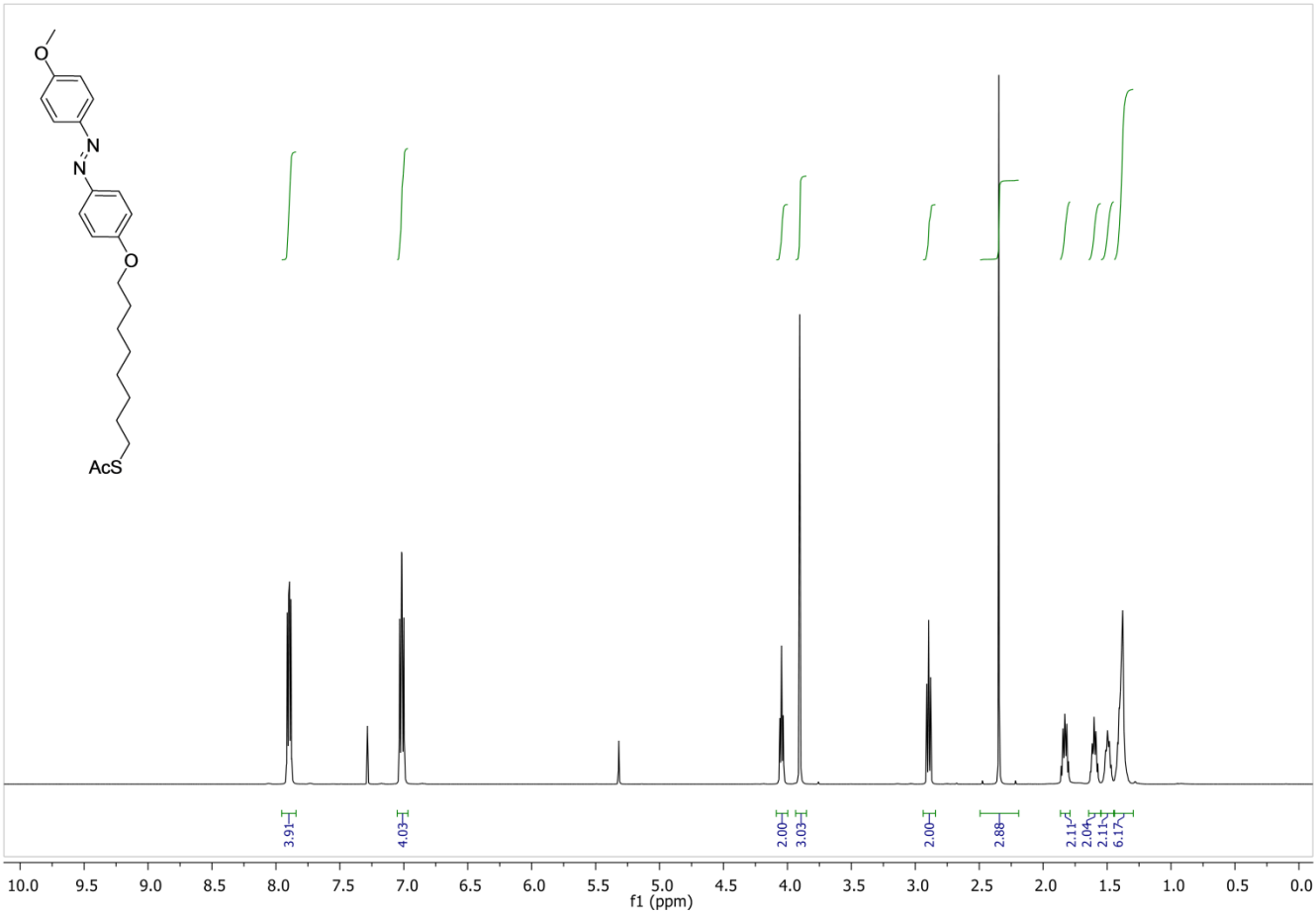

Figure S9 ^{1}H-NMR spectra of compound **4** ($CDCl_3$).

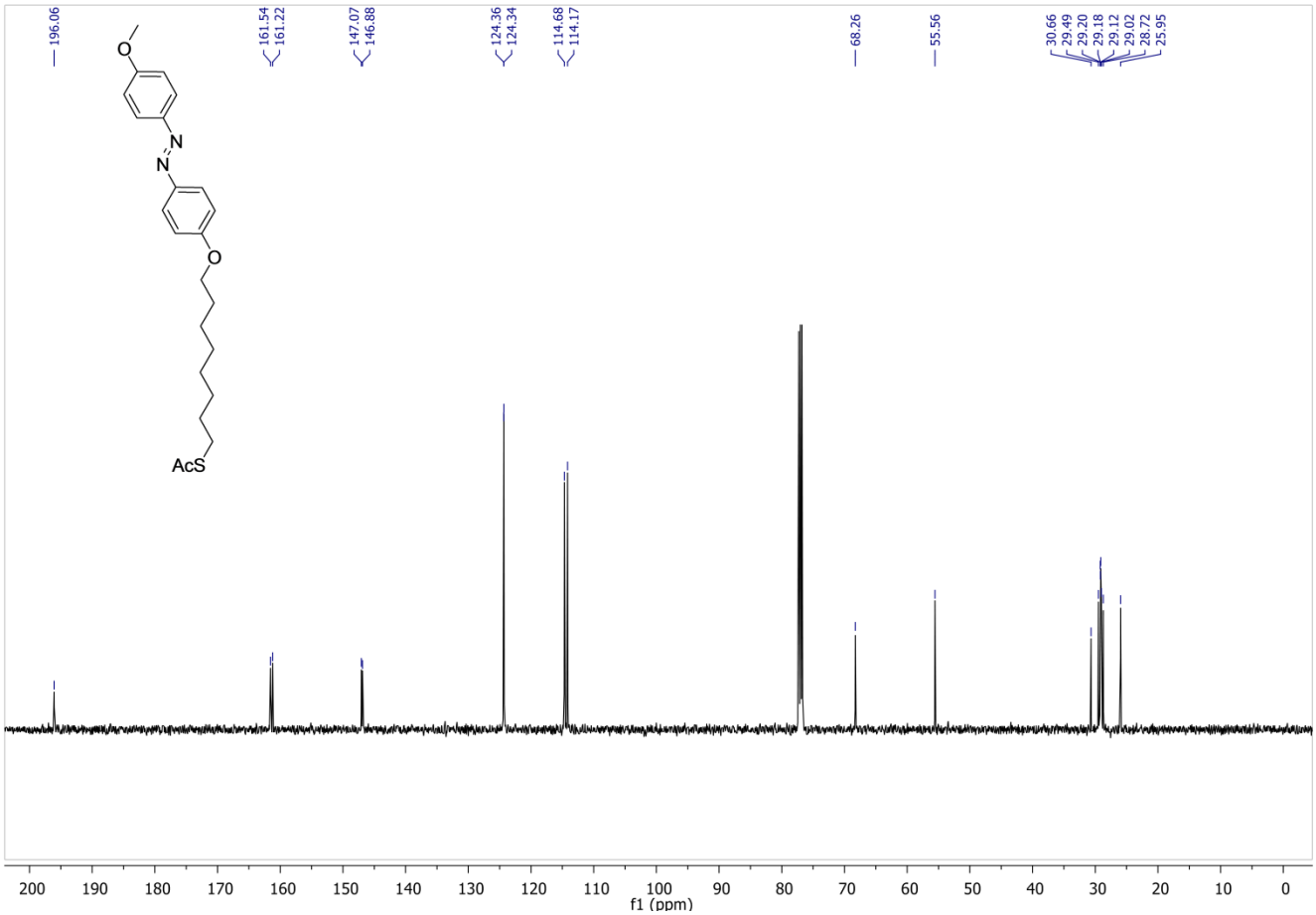

Figure S10 ^{13}C-NMR spectra of compound **4** ($CDCl_3$).

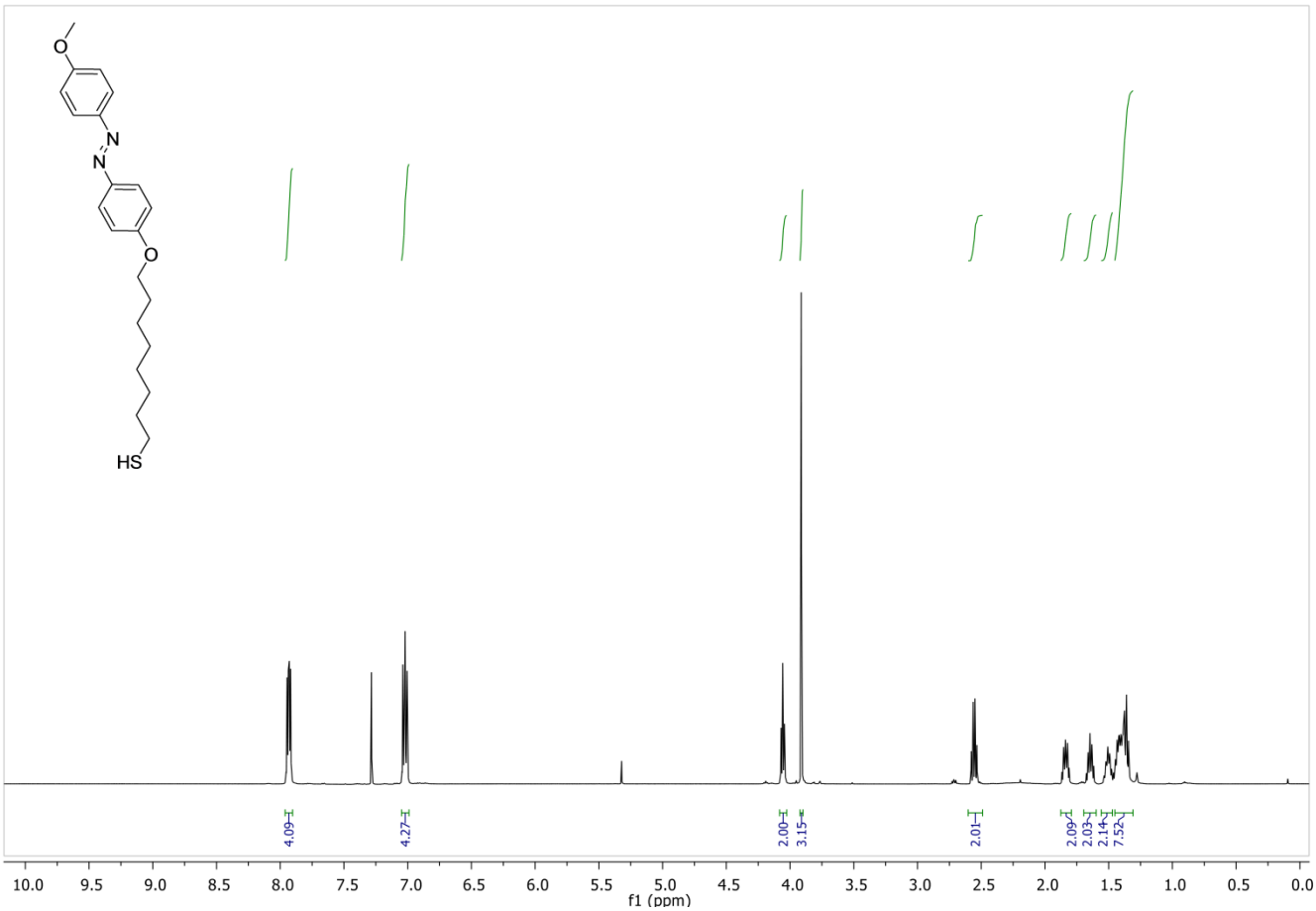

Figure S11 ^{1}H-NMR spectra of compound **5** ($CDCl_3$).

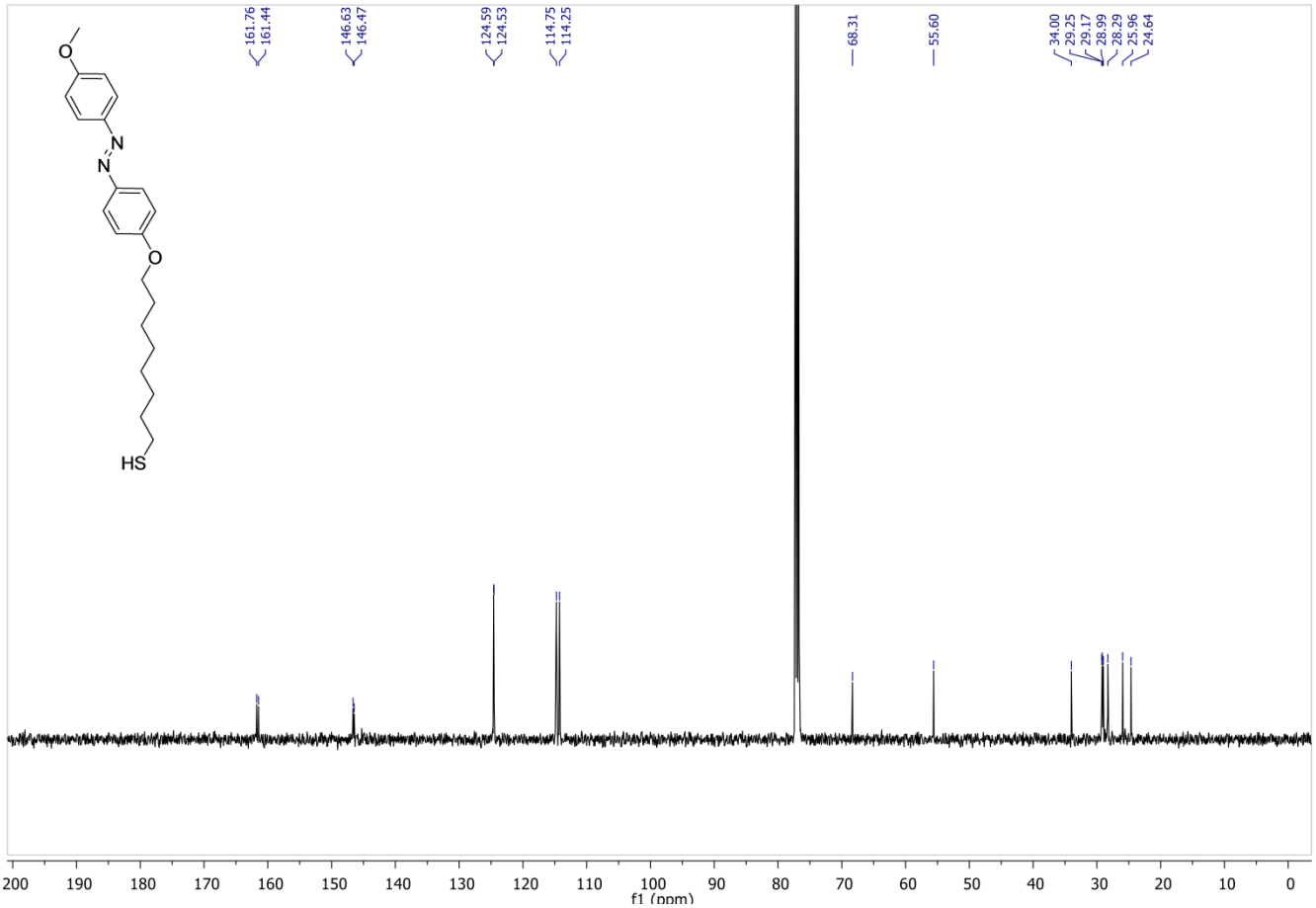

Figure S12 ^{13}C-NMR spectra of compound **5** ($CDCl_3$).

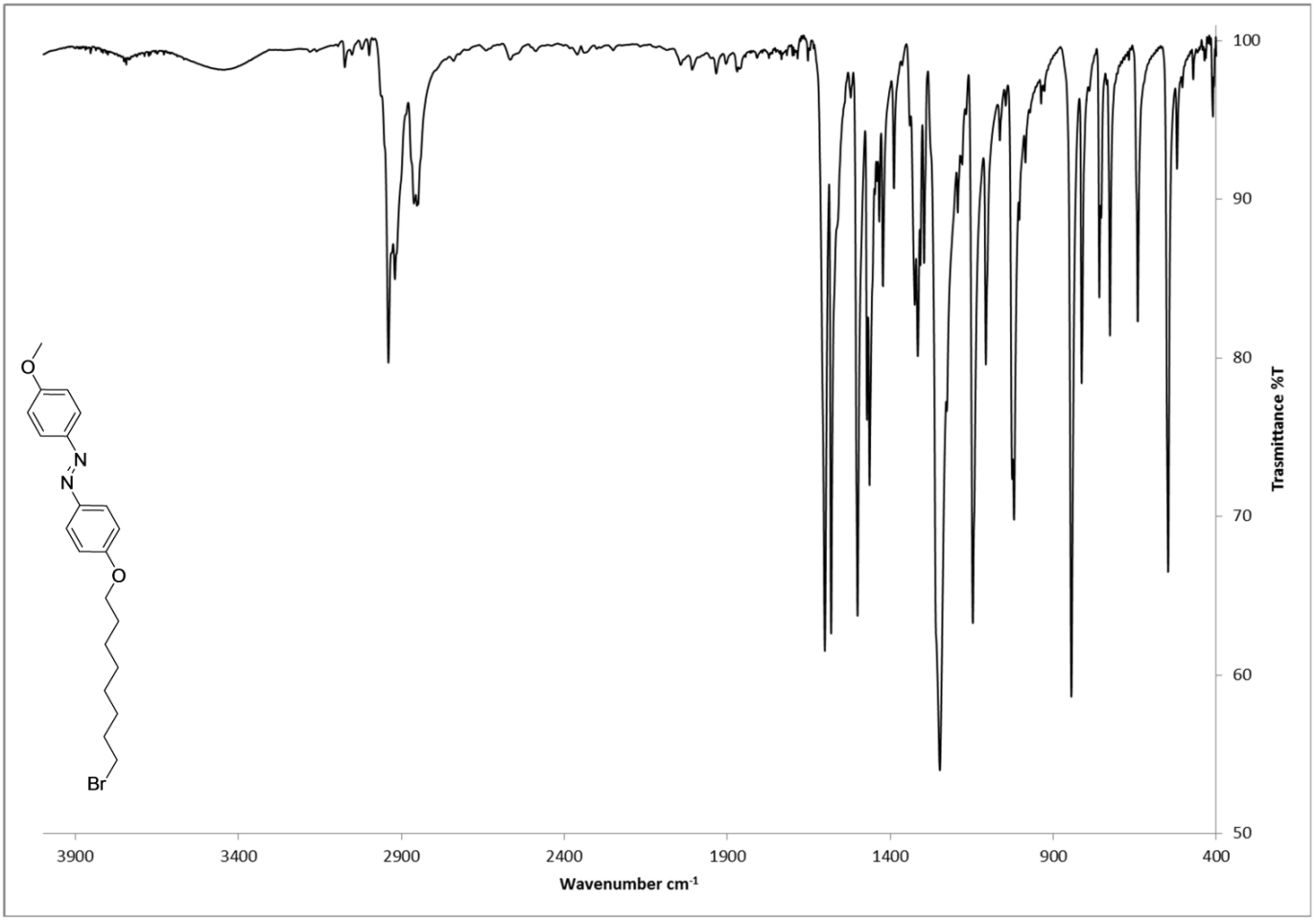

Figure S13 IR spectra of compound **3** (KBr).

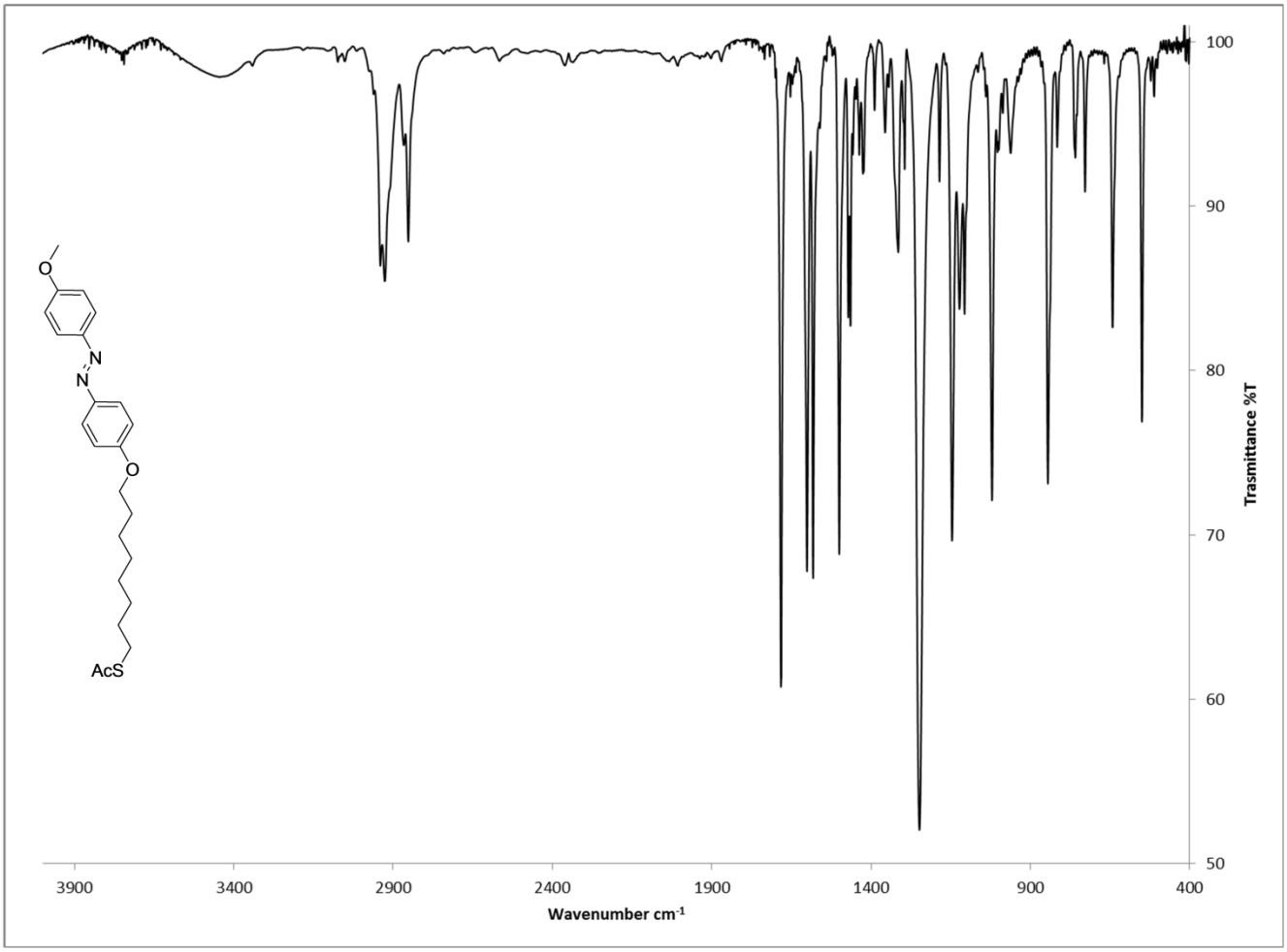

Figure S14 IR spectra of compound **4** (KBr).

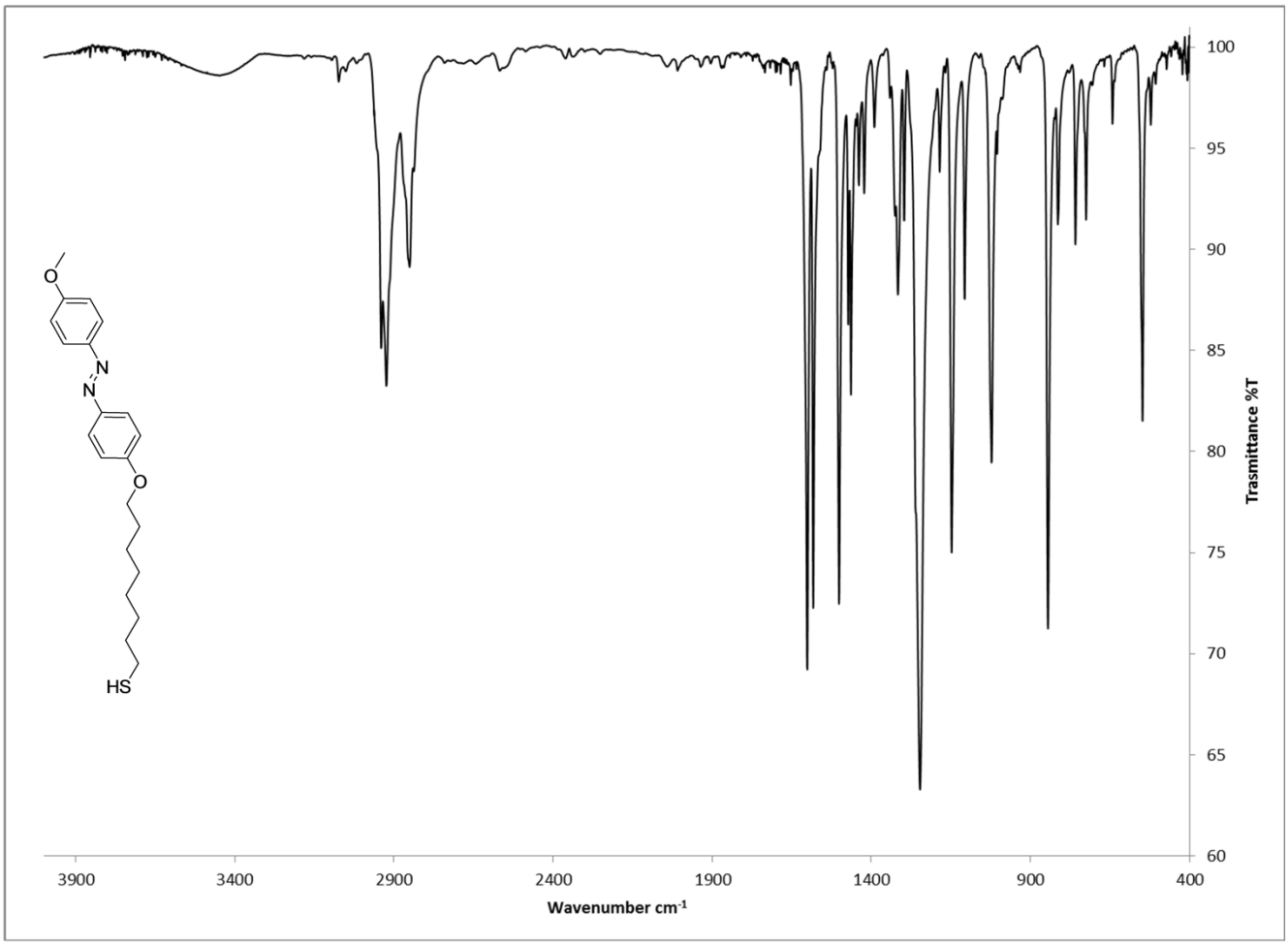

Figure S15 IR spectra of compound **5/*t*A** (KBr).

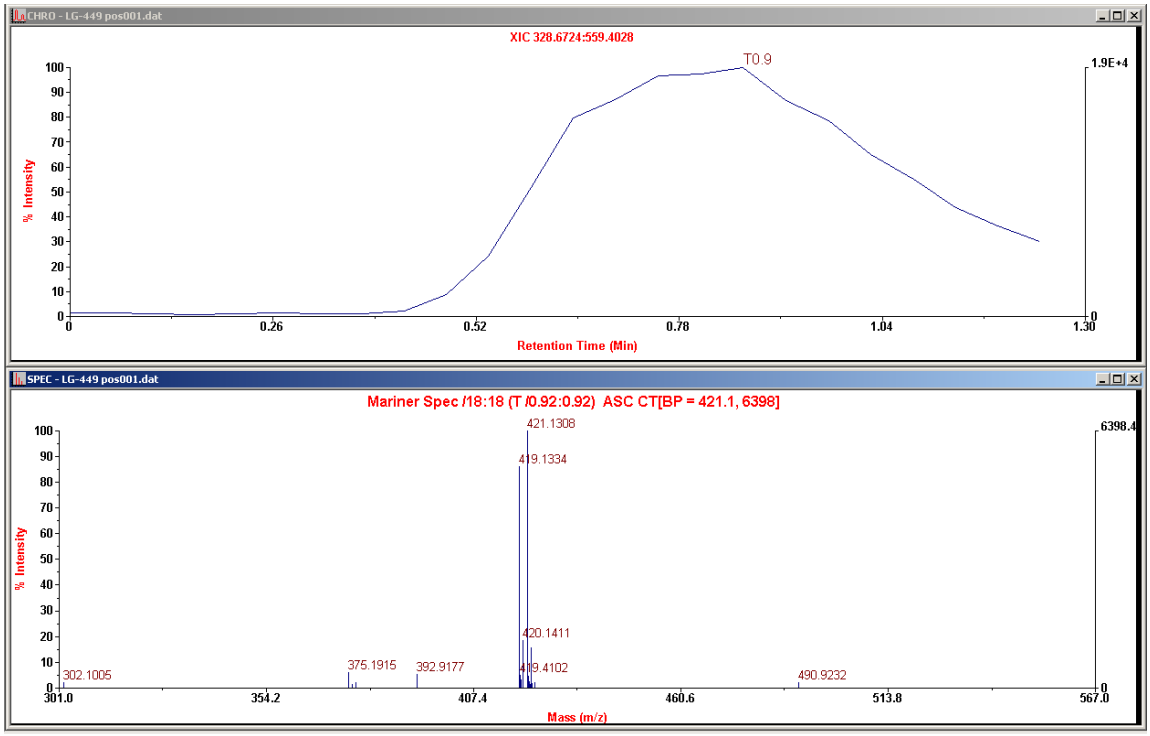

Figure S16 HRMS spectra of compound **3**.

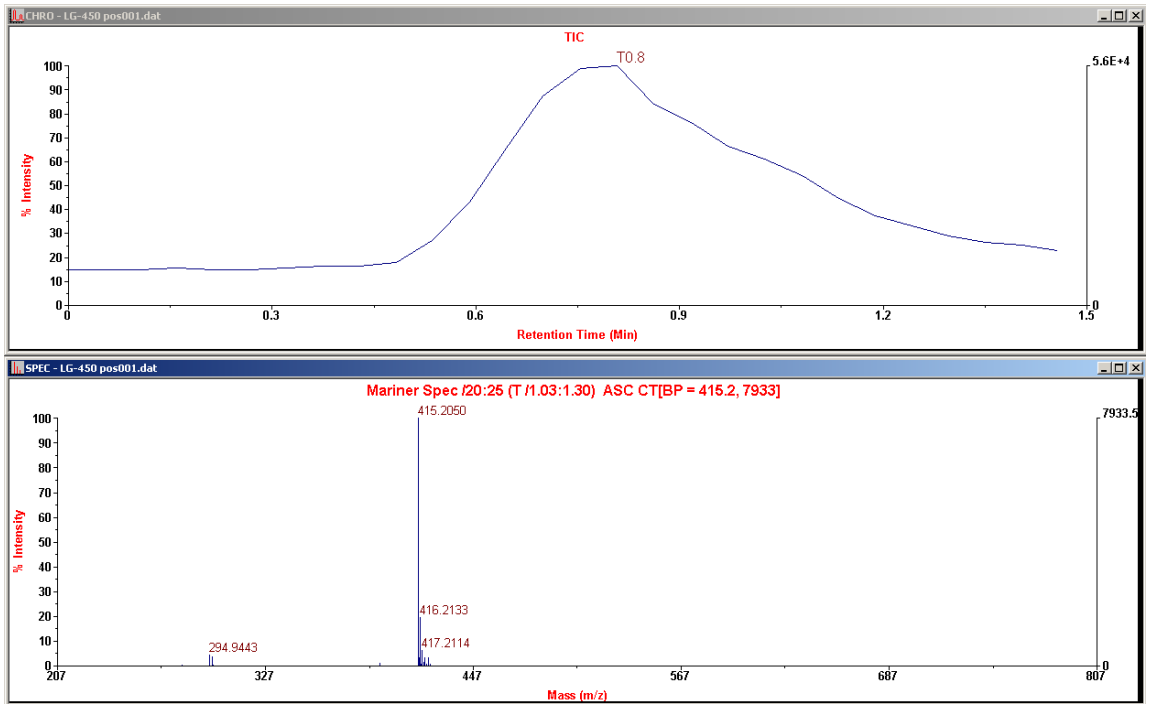

Figure S17 HRMS spectra of compound **4**.

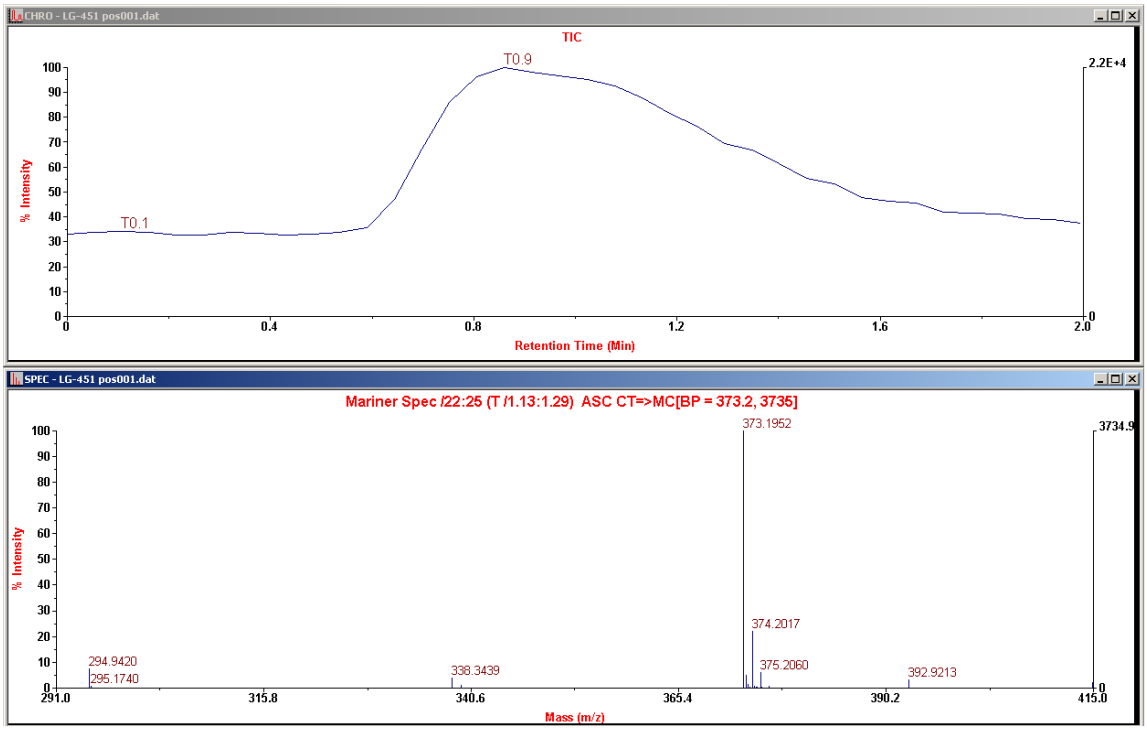

Figure S18 HRMS spectra of compound **5/*t*A**.

8 MD simulations: computational details

Parametrization. Thiolate-protected gold clusters are described using the recently developed unified AMBER-compatible molecular mechanics force field for thiolate-protected gold nanoclusters.[7]

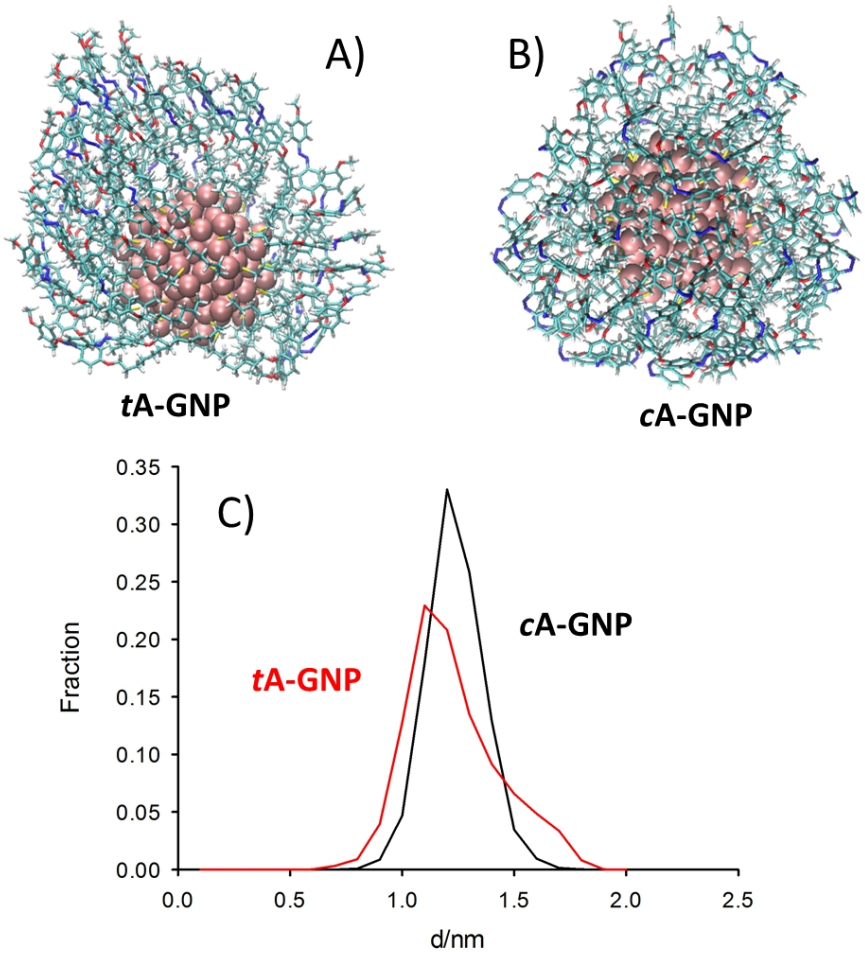

Figure S19 Atomic configuration taken from the last snapshot of MD simulation of A) hair brushed ***t*A-GNP**; B) hair ruffled ***c*A-GNP**; C) normalized radial distribution function averaged over the simulation time of the center of mass of the azobenzene moieties around the gold nanoparticles for ***t*A-GNP** (red line) and ***c*A-GNP** (black line).

The ligand parameters are described using the GAFF force field,[8] the partial charges on the ligand atoms (the S atom was capped by a hydrogen) were optimized following the RESP charge fitting procedure recommended for AMBER. [9] Modified GAFF parameters are used to described correctly the azobenzene *cis* and *trans* geometries.[10]

Geometries. The coordinates of the $Au144(SR)_{60}$ are taken from Ref. [11] and downloaded by Aalto University.[12] The methylthiolates (R=Me) are substituted by the 8-(4-((4-methoxyphenyl)diazenyl)phenoxy)octyl)thiol ligands (compound 5) described in this paper. Two systems are set-up, where the ligands are arranged radially respect to the gold nanoparticle surface, with the same linear alkyl chain geometries, but different *cis*/*trans* configuration of the azobenzene moieties. The thiolate-protected gold clusters are then immersed in a pre-equilbrated chloroform simulation box.

Simulation protocol. About 1000 steps of steepest descent minimization were performed with SANDER. The minimized structure (only cleared from severe sterical clashes) was considered for a 3 step equilibration protocol. Particle Mesh Ewald summation was used throughout (cut off radius of 10 Å for the direct space sum). Individual equilibration steps included

(i) 50 ps of heating to 298 K within an NVT ensemble.

(ii) 50 ps of equilibration MD at 298 K to switch from NVT to NPT and adjust the simulation box. Isotropic position scaling was used at default conditions.

(iii) 400 ps of continued equilibration MD at 298 K for an NPT ensemble

A production MD, with simulation conditions identical to the final equilibration step (iii), was then carried out. Overall sampling time was 50 ns.

Analysis of the trajectory. Using the ptraj module the radial distribution function is calculated over the simulation time. The centers of mass of the azobenzene moieties around the gold nanoparticles for ligands in *trans* and *cis* conformations are considered

9. Energy-tranfer models

Different models have been proposed for energy transfer from a molecular donor to gold NPs.[13] Nevertheless, as a general approach, the ET efficiency (η_{ET}) depends on the distance d and on a critical distance d_0 (which is characteristic of the donor-acceptor pair) according to the equation:

$$\eta_{ET} = 1 - \frac{1}{1 + (\frac{d_0}{d})^n}$$

[Eq. 11]

The exponent *n* changes according to the different theories being *n*=6 for the Forster Resonance Energy Transfer (FRET) model and *n*=4 for the Nano-Surface Energy Transfer (NSET) model.[13a] Other values for *n* has been experimentally determined in the case of GNP used as ET acceptor.[13b] According to Eq. 11, $\eta_{ET} = 0.5$ when $d = d_0$.

As discussed in the main text, independently from the ET model, according to Eq. 11, an increase of d, (as demonstrated by MD simulations results shown in figure S19 going from ***t*A-GNP** to ***c*A-GNP**) makes ET less favored.

If excited state lifetime of the donor (τ_0) and the ET rate constant k_{ET} are considered, η_{ET} can be expressed as:

$$\eta_{ET} = \frac{1}{1 + \frac{k_{ET}}{\tau_0}}$$

[Eq. 12]

According to Eq. 12, for the same k_{ET}, ET efficiency is lower for shorter τ_0. *Cis* AB derivatives have been reported to show much shorter $\tau_0$than *trans* AB isomers.[14]

We would like to stress that these considerations about ET, that partially justify the different behavior of ***t*A-GNP** and ***c*A-GNP**, are only qualitative and that ultrafast transient absorption experiments are in due course to investigate ET in detail.

10. REFERENCES

[1] J. Kim, B. M. Novak, A. J. Waddon, *Macromolecules* **2004**, *37*, 8286-8292.
[2] F. Manea, C. Bindoli, S. Polizzi, L. Lay, P. Scrimin, *Langmuir* **2008**, *24*, 4120-4124.
[3] a) N. K. Chaki, Y. Negishi, H. Tsunoyama, Y. Shichibu, T. Tsukuda, *J. Am. Chem. Soc.* **2008**, *130*, 8608-+; b) H. Qian, R. Jin, *Nano Lett.* **2009**, *9*, 4083-4087.
[4] L. M. Tvedte, C. J. Ackerson, *J. Phys. Chem. A* **2014**, *118*, 8124-8128.
[5] M. Montalti, A. Credi, L. Prodi, M. T. Gandolfi, *Handbook of photochemistry*, CRC press, **2006**.
[6] G. Zimmerman, L.-Y. Chow, U.-J. Paik, *J. Am. Chem. Soc.* **1958**, *80*, 3528-3531.
[7] E. Pohjolainen, X. Chen, S. Malola, G. Groenhof, H. Häkkinen, *J. Chem. Theory Comput.* **2016**, *12*, 1342-1350.
[8] J. Wang, R. M. Wolf, J. W. Caldwell, P. A. Kollman, D. A. Case, *J. Comput. Chem.* **2004**, *25*, 1157-1174.
[9] C. I. Bayly, P. Cieplak, W. Cornell, P. A. Kollman, *J. Phys. Chem.* **1993**, *97*, 10269-10280.
[10] P. Duchstein, C. Neiss, A. Görling, D. Zahn, *J. Mol. Model.* **2012**, *18*, 2479-2482.
[11] O. Lopez-Acevedo, J. Akola, R. L. Whetten, H. Grönbeck, H. Häkkinen, *J. Phys. Chem. C* **2009**, *113*, 5035-5038.
[12] https://wiki.aalto.fi/display/CSM/Coordinates.
[13] a) T. L. Jennings, M. P. Singh, G. F. Strouse, *J. Am. Chem. Soc.* **2006**, *128*, 5462-5467; b) A. Samanta, Y. D. Zhou, S. L. Zou, H. Yan, Y. Liu, *Nano Lett.* **2014**, *14*, 5052-5057.
[14] H. M. D. Bandara, S. C. Burdette, *Chem. Soc. Rev.* **2012**, *41*, 1809-1825.